SUMMARY OF PROFESSIONAL ACCOMPLISHMENTS

1 NAME

Maciej Krzysztof Lisicki

2 DIPLOMAS, DEGREES CONFERRED IN SPECIFIC AREAS OF SCIENCE OR ARTS

- **Ph.D. degree in Physics**
  Date: 29 September 2015
  Thesis title: *Evanescent wave scattering by optically anisotropic Brownian particles*
  Supervisor: prof. dr hab. Bogdan Cichocki
  Research unit: Faculty of Physics, University of Warsaw

- **M.Sc. degree in Physics**
  Date: 29 April 2011
  Thesis title: *One-particle correlation function in evanescent wave dynamic light scattering*
  Supervisor: prof. dr hab. Bogdan Cichocki
  Research unit: Faculty of Physics, University of Warsaw

3 INFORMATION ON EMPLOYMENT IN RESEARCH INSTITUTES OR FACULTIES/DEPARTMENTS

- **Assistant Professor**, since February 2019
  Faculty of Physics, University of Warsaw

- **Postdoctoral Research Associate**, grudzień 2015 – styczeń 2019
  University of Cambridge, Cambridge, United Kingdom

- **Visiting Scientist, David Crighton Fellow**, September – December 2015
  University of Cambridge, Cambridge, United Kingdom

- **Visiting Scientist**, April 2011 – April 2014
  Forschungszentrum Jülich, Germany

- **Ph.D. Student**, June 2011 – September 2015
  Faculty of Physics, University of Warsaw

4 DESCRIPTION OF THE ACHIEVEMENTS, SET OUT IN ART. 219 PARA 1 POINT 2 OF THE ACT

A. TITLE OF THE SCIENTIFIC ACHIEVEMENT

A series of scientific articles related thematically entitled
Anisotropy of hydrodynamic interaction in confined geometry

B. LIST OF PUBLICATIONS FORMING THE SCIENTIFIC ACHIEVEMENT (reverse chronological order)

[A1] R. Waszkiewicz, **M. Lisicki**†,
Hydrodynamic effects in the capture of rod-like molecules by a nanopore,
J. Phys. Condens. Matter **33**, 104005 (2021). († corresponding author)

[A2] A. Daddi-Moussa-Ider*, **M. Lisicki***, A.J.T.M. Mathijssen*,
Surface rheotaxis of three-sphere microrobots with cargo,
Phys. Rev. Applied **14**, 024071 (2020). (* equal author contributions)

[A3] H.R. Vutukuri, **M. Lisicki**, E. Lauga, J. Vermant,
Light-switchable propulsion of active particles with reversible interactions,
Nat. Commun. **11**, 2628 (2020).

[A4] A. Daddi-Moussa-Ider, **M. Lisicki**, S. Gekle, A. M. Menzel, H. Löwen
Hydrodynamic coupling and rotational mobilities near planar elastic membranes,
J. Chem. Phys. **149**, 014901 (2018). Selected as *JCP Editor's Choice 2018*.

[A5] A. Daddi-Moussa-Ider, **M. Lisicki**, A.J.T.M. Mathijssen, C. Hoell, S. Goh, J. Bławzdziewicz, A. M. Menzel, H. Löwen,
State diagram of a three-sphere microswimmer in a channel,
J. Phys.: Condens. Matter **30**, 254004 (2018).

[A6] A. Daddi-Moussa-Ider, **M. Lisicki**, C. Hoell, H. Löwen,
Swimming trajectories of a three-sphere microswimmer near a wall,
J. Chem. Phys. **148**, 134904 (2018).

[A7] L. Koens*, **M. Lisicki***, E. Lauga,
The non-Gaussian tops and tails of diffusing boomerangs,
Soft Matter **13**, 2977 (2017). (* equal author contributions)

[A8] A. Daddi-Moussa-Ider*, **M. Lisicki***, S. Gekle
Mobility of an axisymmetric particle near an elastic interface,
J. Fluid Mech. **811**, 210 (2017). (* equal author contributions)

[A9] **M. Lisicki**, B. Cichocki, E. Wajnryb,
Near-wall diffusion tensor of an axisymmetric colloidal particle,
J. Chem. Phys. **145**, 034904, (2016).

Detailed information about my contribution to the articles above is collected in Załącznik nr 4 (Appendix 4).

C. DESCRPTION OF THE SCIENTIFIC ACHIEVEMENT

Introduction

Soft, colloidal, and active matter systems remain a vibrant topic of research within the scientific community. This is partly related to the increasing attention being devoted to multidisciplinary problems at the interface between physics, chemistry, biology, and engineering. Research methods originating from physics are being profitably applied to study complex biological systems, both in terms of theoretical and numerical modelling, as well as using cutting-edge experimental techniques which give us insights into the level of details unseen before.

Most of the aforementioned systems reside in an aqueous or fluid environment. Given their small spatial sizes of the order of micrometers, the typical Reynolds number describing the flow is vanishingly small, and therefore the dynamics are dominated by viscosity effects. Although equilibrium properties of suspensions and structured fluids are now relatively well understood [1–3], elucidating the dynamics still remains a challenge, particularly in biological and active matter, where the processes are inherently non-equilibrium [4]. Stokes flows are known for their long-range and many-body character. In order to account for flow and diffusion in microscale systems, one must therefore explore hydrodynamic interactions (HI) between its constitutive elements [5, 6].

Viscous flows are also known to be strongly influenced by the effects of confinement [7]. The presence of boundaries in the system introduces anisotropy of HI which become directional. If an object immersed in a fluid is anisotropic, these effects couple in a non-trivial way, giving rise to a number of interesting dynamical features.

The presented works **[A1–A9]** discuss the anisotropy of hydrodynamic interactions in systems confined by boundaries. They encompass a general theoretical description of flow in restricted geometry and also apply this theoretical approach to elucidate the observed dynamical features of particular, experimentally relevant systems. In each case, a model is developed basing on the Stokes equation for the fluid flow, and taking into account specific experimental details in order to provide an interpretation to the data collected. All works presented here focus on wall-bounded geometry, where a planar boundary introduces a pronounced increase in hydrodynamic drag for objects in its proximity, but also changes the directionality of HI. We can distinguish four main broad areas of research which are intertwined within the research works included in the Achievement:

(i) Near-wall hydrodynamics of axisymmetric particles **[A1-A6, A8, A9]**.

(ii) Elastohydrodynamic effects in confinement **[A4, A8]**.

(iii) Active transport and artificial microswimmers in confinement **[A2-A6]**.

(iv) Diffusive transport in restricted geometry **[A1, A4-A9]**.

The structure of the description is as follows. Section 1 is an introduction to the theoretical methods used to describe hydrodynamic interactions in Stokes flows. Section 2 describes the results contained within **[A1-A9]**. It is divided into four parts described above. For each of these topics, a broader context and introduction is given, after which we discuss the papers in detail. In part (i) we include **[A1, A9]**; part (ii) describes Refs. **[A4, A8]**; part (iii) is focused on Ref. **[A3]** which is a joint theoretical-experimental work and separately Refs. **[A2, A5, A6]** devoted to theoretical considerations; part (iv) concerns Ref. **[A7]**. The concluding Section 3 summarises the presentation. Additionally, a general overview of the problem of HI in active and passive microscale systems is given in a review chapter **[B9]**, of which I am the main author.

1. Hydrodynamic interactions in Stokes flows

Boundaries and interfaces play an important role in the colloidal world. Many relevant biological, industrial, and diagnostic processes involve flow either in channels, or close to surfaces [8–10]. Many examples of such processes are given in the following parts of the text. Geometric confinement introduces anisotropy in the diffusive motion of sub-micron particles, and the presence of neighbouring walls increases the drag force experienced by colloidal particles [7]. In this context, the central quantity is the hydrodynamic mobility tensor $\boldsymbol{\mu}$, which is related to the diffusion tensor $\boldsymbol{D}$ by the fluctuation-dissipation theorem [11]

$$\boldsymbol{D} = k_B T \boldsymbol{\mu}. \tag{1}$$

On the colloidal length scales and for time scales typical for microparticles or microscopic swimming microorganisms, the flow field around a particle in a Newtonian fluid of viscosity η is aptly described by the incompressible Stokes equations [12]

$$\eta \nabla^2 \boldsymbol{v}(\boldsymbol{r}) - \nabla p(\boldsymbol{r}) = -\boldsymbol{f}(\boldsymbol{r}), \qquad \nabla \cdot \boldsymbol{v}(\boldsymbol{r}) = 0, \tag{2}$$

where $\boldsymbol{f}(\boldsymbol{r})$ is the force density the particle exerts on the fluid when subjected to flow, and $p(\boldsymbol{r})$ is the pressure field. The flow caused by the presence of a particle can be superposed with an ambient flow $\boldsymbol{v}_0(\boldsymbol{r})$, with the vorticity and rate of strain defined as $\boldsymbol{\omega}_0(\boldsymbol{r}) = \frac{1}{2}\nabla \times \boldsymbol{v}_0(\boldsymbol{r})$ and $\boldsymbol{E}_0(\boldsymbol{r}) = \overline{\nabla \boldsymbol{v}_0(\boldsymbol{r})}$, respectively, with the bar denoting the symmetric and traceless part.

Given the force density, one can calculate the force $\boldsymbol{F}$, torque $\boldsymbol{T}$, and symmetric dipole moment (stresslet) $\boldsymbol{S}$ exerted by the fluid on the particle by integration over the particle surface. In result of the external flow, motion is induced, and the particle gains linear and angular velocities, $\boldsymbol{V}$ and $\boldsymbol{\Omega}$, respectively. Owing to the linearity of the Stokes equations, we deduce that the force moments $\boldsymbol{F}$, $\boldsymbol{G}$ and $\boldsymbol{S}$, are linearly related to the velocity moments via the generalised friction (or resistance) tensor [12, 13]

$$\begin{pmatrix} \boldsymbol{F} \\ \boldsymbol{T} \\ \boldsymbol{S} \end{pmatrix} = \begin{pmatrix} \boldsymbol{\zeta}^{tt} & \boldsymbol{\zeta}^{tr} & \boldsymbol{\zeta}^{td} \\ \boldsymbol{\zeta}^{rt} & \boldsymbol{\zeta}^{rr} & \boldsymbol{\zeta}^{rd} \\ \boldsymbol{\zeta}^{dt} & \boldsymbol{\zeta}^{dr} & \boldsymbol{\zeta}^{dd} \end{pmatrix} \begin{pmatrix} \boldsymbol{v}_0(\boldsymbol{r}) - \boldsymbol{V} \\ \boldsymbol{\omega}_0(\boldsymbol{r}) - \boldsymbol{\Omega} \\ \boldsymbol{E}_0(\boldsymbol{r}) \end{pmatrix}. \tag{3}$$

Here we have decomposed the generalised friction tensor into 9 sub-matrices. The indices tt and rr denote the translational and rotational parts, respectively. The tensors $\boldsymbol{\zeta}^{tr}$ and $\boldsymbol{\zeta}^{rt}$ describe the translation-rotation coupling, and the d-tensors describe the response to an external straining flow. In most cases, however, one considers a 6×6 friction matrix $\boldsymbol{\zeta}$ relating the force and torque to linear and angular velocities. The additional d elements turn out to be essential for the calculation of the correction to the friction matrix in the presence of a wall, hence we include them here. In a reversed problem, when the forces and torques are known, and the particle motion is sought, the relationship between them is given by the mobility tensor $\boldsymbol{\mu}$ which is the inverse of the friction tensor

$$\boldsymbol{\mu} = \begin{pmatrix} \boldsymbol{\mu}^{tt} & \boldsymbol{\mu}^{tr} \\ \boldsymbol{\mu}^{rt} & \boldsymbol{\mu}^{rr} \end{pmatrix} = \begin{pmatrix} \boldsymbol{\zeta}^{tt} & \boldsymbol{\zeta}^{tr} \\ \boldsymbol{\zeta}^{rt} & \boldsymbol{\zeta}^{rr} \end{pmatrix}^{-1} = \boldsymbol{\zeta}^{-1}. \tag{4}$$

In a bulk system, the mobility tensor and the friction tensor, denoted by $\boldsymbol{\mu}_0$ and $\boldsymbol{\zeta}_0$, respectively, do not depend on the position of the particle due to translational invariance. The situation is different if a confining boundary is present, since the symmetry is broken and the hydrodynamic tensors depend both on the distance to the boundary, and on the relative orientation of the particle with respect to the surface.

The notion of friction and mobility tensors is easily extended to many particles [12, 13]. In this case, the so-called grand mobility (friction) tensor relates the forces and torques with velocities of all the particles. It encodes complete information on the dynamics of a suspension. Since the hydrodynamic interaction are long-ranged and have a many-body character, the calculation of $\boldsymbol{\mu}$ is often a challenge. On the other hand, a number of techniques are available to calculate the hydrodynamic tensors.

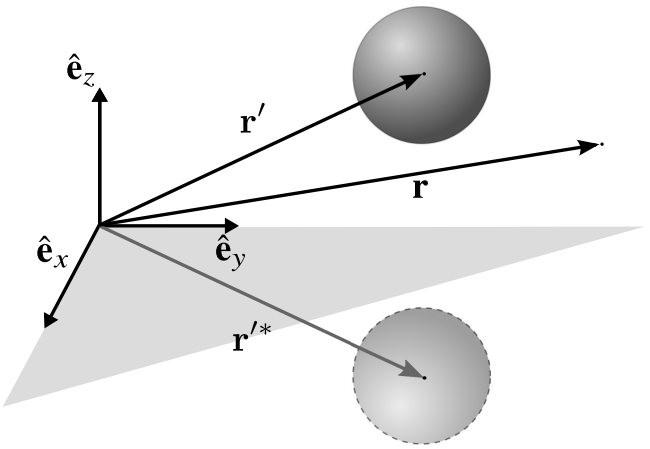

Figure 1: The image sphere for a spherical particle in the presence of a boundary which may be either a free slip surface, or a hard no-slip wall.

The simplest approach relies on approximating the particles as point-like objects. Owing to the linearity of the Stokes equations, we can introduce a Green's function, which for a point-force in an unbounded domain is the well-known Oseen tensor [5, 12, 14]. For force placed at the origin, it takes the form

$$\boldsymbol{G}_0(\boldsymbol{r}) = \frac{1}{8\pi\eta r}\left(\mathbf{1} + \hat{\boldsymbol{r}}\hat{\boldsymbol{r}}\right), \tag{5}$$

with $r = |\boldsymbol{r}|$ and $\hat{\boldsymbol{r}} = \boldsymbol{r}/r$. In the Oseen approximation, the mobilities of particles are calculated from the point-force solutions, combined with the Stokes mobility $\mu_0 = 1/6\pi\eta a$ for a particle of radius a. This approach, however, produces mobility matrices that might not be positive-definite, as required by the second law of thermodynamics. However, more accurate approximations which assure this property are available, starting from the Rotne-Prager-Yamakawa tensors [15–18], through Stokesian Dynamics models [19], to precise multipole methods which rely on decomposing a flow field around the particles into a complete set of solutions of the Stokes equations, and taking into account appropriate boundary conditions on the surfaces of the particles, as detailed out in the review by Ekiel-Jeżewska & Wajnryb [13]. For all of these schemes, starting from the appropriate form of the Green's tensor for a given geometry, is a crucial modelling step.

In the presence of system boundaries, it is convenient to decompose the full Green's tensor into the Oseen tensor $\boldsymbol{G}_0$ and the part describing the flow reflected from interfaces

$$\boldsymbol{G}(\boldsymbol{r}, \boldsymbol{r}') = \boldsymbol{G}_0(\boldsymbol{r} - \boldsymbol{r}') + \boldsymbol{\Delta G}(\boldsymbol{r}, \boldsymbol{r}'). \tag{6}$$

In general, the Green's tensor describes the flow at a point $\boldsymbol{r}$ due to a source (point force) acting on the fluid at a point $\boldsymbol{r}'$. For a fluid bounded by a planar hard wall, or a free surface, a closed form of the Green's tensor $\boldsymbol{G}$ is known. To present it, we assume the geometry as sketched in Fig. 1, with the fluid in the upper half-space $z > 0$ bounded by a planar wall at $z = 0$. We also introduce the reflection operator $\boldsymbol{P} = \mathbf{1} - \hat{\boldsymbol{e}}_z\hat{\boldsymbol{e}}_z$, which transforms any point $\boldsymbol{r}$ into its mirror image $\boldsymbol{r}^*$ with respect to the wall. For a free surface, at which the normal velocity and tangential stress vanish, the Green's tensor reads [20]

$$\boldsymbol{G}_f(\boldsymbol{r}, \boldsymbol{r}') = \boldsymbol{G}_0(\boldsymbol{r} - \boldsymbol{r}') + \boldsymbol{\Delta G}_f(\boldsymbol{r}, \boldsymbol{r}') = \boldsymbol{G}_0(\boldsymbol{r} - \boldsymbol{r}') + \boldsymbol{G}_0(\boldsymbol{r} - \boldsymbol{r}'^*) \cdot \boldsymbol{P}, \tag{7}$$

which has an elegant interpretation that for a point force (called a Stokeslet), the additional (reflected) velocity field near a free surface is equivalent to that of another Stokeslet placed at its mirror image location. For a hard no-slip wall, the Green tensor (also called the Blake tensor) has been found by Lorentz in 1907 [21] as

$$\begin{aligned}\boldsymbol{G}_w(\boldsymbol{r}, \boldsymbol{r}') = \boldsymbol{G}_0(\boldsymbol{r} - \boldsymbol{r}') + \boldsymbol{\Delta G}_w(\boldsymbol{r}, \boldsymbol{r}') = \boldsymbol{G}_0(\boldsymbol{r} - \boldsymbol{r}') - \boldsymbol{G}_0(\boldsymbol{r} - \boldsymbol{r}'^*) \cdot \boldsymbol{P} \\ - 2z_0\hat{\boldsymbol{e}}_z \cdot \boldsymbol{G}_0(\boldsymbol{r} - \boldsymbol{r}'^*)\overleftarrow{\boldsymbol{\nabla}}_{\boldsymbol{r}} \cdot \boldsymbol{P} + z_0^2\nabla_{\boldsymbol{r}}^2\boldsymbol{G}_0(\boldsymbol{r} - \boldsymbol{r}'^*) \cdot \boldsymbol{P},\end{aligned} \tag{8}$$

where $[\boldsymbol{a}\overleftarrow{\boldsymbol{\nabla}}_{\boldsymbol{r}}]_{\alpha\beta} = \frac{\partial}{\partial \boldsymbol{r}_\beta}\boldsymbol{a}_\alpha$ and $z_0 = \boldsymbol{r}'\cdot\boldsymbol{e}_z$ being the height of the source above the wall. This expression can be rewritten in other ways, as e.g. in Refs. [22–24], which give it a simple interpretation. Here, the image system for a Stokeslet involves additional terms, the so-called Stokeslet doublet and source doublet [22], which have a different directional character than a Stokeslet. The solution for the no-slip wall, termed the Blake tensor, is fundamental for many works concerning near-interface hydrodynamics [25–32]. Similar results for the Green's function for an interface separating two fluids have also been derived [33–36], also for partial slip boundary conditions [37–39], and for thin films [40–42]. Many of the early results are summarised in the excellent monograph of Happel and Brenner [7].

2. Description of results

Near-wall dynamics of axisymmetric particles

In Article **[A9]**, we describe the dynamics of an axially symmetric colloidal particle close to a planar no-slip boundary. The paper is co-authored by B. Cichocki and E. Wajnryb. It is motivated by the need to describe and interpret the dynamics of complex-shaped particles near interfaces. Recent years have brought significant advancement in experimental techniques which allow to explore near-wall dynamics in detail, using optical microscopy [43–48] and light scattering tools, such as evanescent wave dynamic light scattering [49–51]. The latter is now a well-established tool which has profitably been used to investigate translational **[B13]** and rotational diffusion **[B12, B11]** of spherical colloids in dilute suspensions. Due to the complex nature of the experiments, available experimental data for non-spherical particles such as dumbbells [52, 53] or rods are still lacking proper interpretation. It is therefore particularly important in this context to understand the nature of hydrodynamic interactions of an axially symmetric particle with a wall, and has partially motivated this work. Axisymmetric particles moving close to a boundary experience an additional anisotropic drag force on top of their own friction anisotropy stemming from their non-spherical shape. This coupling leads to a complicated behaviour, observed e.g. in simulations of such particles sedimenting next to a vertical wall [54, 55], with the mobility of the particle depending on its position and orientation. Available predictions for the near-wall mobility of an axisymmetric particle mostly feature a slender-body approach, yielding rather complex results for general wall-particle orientations near a solid boundary [56] or near a fluid interface [57]. These predictions were analysed in detail in the context of sedimentation in several special alignments [58]. On the other hand, previous numerical works involve the boundary integral method [59], finite element method [60] or stochastic rotation dynamics [61] from which empirical relations are extracted. The lack of theoretical predictions for the near-wall mobility of a rod-shaped and non-slender particle in an arbitrary configuration requires the use of more precise numerical methods. A possible way is to use advanced algorithms involving bead-models which take into account lubrication when the particles come close to the interface [23], which are rather costly. Earlier numerical works suggested that the near-wall mobility (or diffusion) matrix depends on the distance and orientation of the particle in a form that is easily approximated by low-order polynomials in the orientational angle θ (being the angle between the particle axis and the wall-normal direction) [61].

An exemplary system analysed in this work is depicted in Fig. 2. In order to investigate these claims and provide a theoretical foundation, in Ref. **[A9]** we have examined in detail the structure of the near-wall mobility matrix of an axisymmetric colloid by analysing the leading-order terms in the multipole expansion of the Blake tensor. In the presence of the wall, the friction tensor of an axisymmetric particle has the form

$$\boldsymbol{\zeta} = \boldsymbol{\zeta}_0 + \boldsymbol{\Delta\zeta}, \tag{9}$$

where $\boldsymbol{\zeta}_0$ is the bulk friction tensor. In **[A9]**, we derived explicit analytical formulae for the leading-order correction $\boldsymbol{\Delta\zeta}$ to the bulk friction tensor of an axisymmetric particle due to the presence of a wall. The

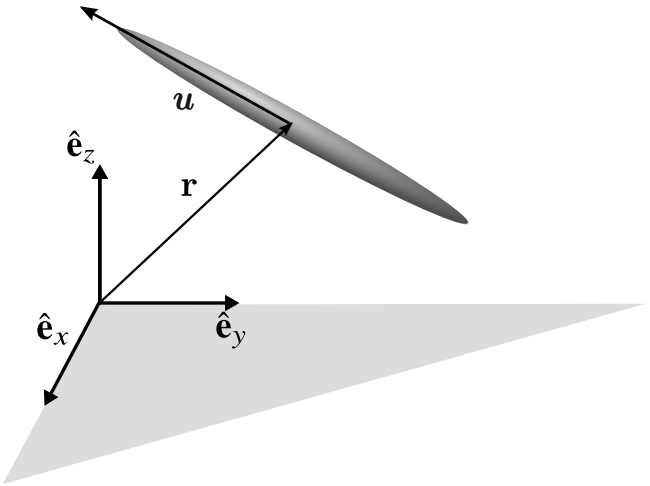

Figure 2: An axially symmetric colloidal particle near a planar hard wall. The director of the particle is $\boldsymbol{u}$. The hydrodynamic mobility of the rod-like colloid depends on the wall-particle distance $H = \hat{\boldsymbol{e}}_z \cdot \boldsymbol{r}$ and the polar angle $\cos\theta = \boldsymbol{u} \cdot \hat{\boldsymbol{e}}_z$.

correction has a particularly elegant form

$$\boldsymbol{\Delta\zeta}_w^{tt} = -\frac{\boldsymbol{A}_1(\boldsymbol{\zeta}_0,\theta)}{2H} + \frac{\boldsymbol{A}_2(\boldsymbol{\zeta}_0,\theta)}{(2H)^2} + \mathcal{O}(H^{-3}), \tag{10a}$$

$$\boldsymbol{\Delta\zeta}_w^{tr} = -\frac{\boldsymbol{B}(\boldsymbol{\zeta}_0,\theta)}{(2H)^2} + \mathcal{O}(H^{-3}), \tag{10b}$$

$$\boldsymbol{\Delta\zeta}_w^{rt} = -\frac{(\boldsymbol{B}(\boldsymbol{\zeta}_0,\theta))^{\mathrm{T}}}{(2H)^2} + \mathcal{O}(H^{-3}), \tag{10c}$$

$$\boldsymbol{\Delta\zeta}_w^{rr} = -\frac{\boldsymbol{C}(\boldsymbol{\zeta}_0,\theta)}{(2H)^3} + \mathcal{O}(H^{-4}). \tag{10d}$$

We derive the tensors $\boldsymbol{A}_{1,2}$, $\boldsymbol{B}$, $\boldsymbol{C}$ above from the multipole expansion of the Blake tensor [22] (Oseen tensor for the wall-bounded geometry) and they depend on the bulk components of the friction tensor of a rod-like particle, $\boldsymbol{\zeta}_0$, and its orientation angle θ but not on the wall-particle distance. The dominant power of $1/H$ depends on the component in question (translational, rotational, or coupling friction matrix) and its angular structure is represented by low-order polynomials in sines and cosines of the particle's inclination angle to the wall. Our results provide a practical, analytical approximation for translational and rotational motion, as well as the translation-rotation coupling tensors. The near-wall mobility $\boldsymbol{\mu}$ (or diffusivity $\boldsymbol{D} = k_B T\boldsymbol{\mu}$) are then obtained by inverting the corrected single-particle friction matrix, as

$$\boldsymbol{\mu} = \boldsymbol{\zeta}^{-1} = (\boldsymbol{\zeta}_0 + \boldsymbol{\Delta\zeta})^{-1}. \tag{11}$$

We also discuss the leading-order formulae for mobility not being as accurate a representation as the numerically inverted leading-order expressions for friction. Our findings provide a simple approximation to the anisotropic diffusion tensor near a wall, which completes and corrects relations known from earlier numerical and theoretical findings. The input required to evaluate the correction is the bulk friction matrix of the particle. For simple axisymmetric shapes, such as ellipsoids, these coefficients are known analytically [12]. For more complex shapes, they can be obtained e.g. from widely available bead-model calculators, such as GRPY [18] or HYDRO++ [62]. Our results compare favourably with the predictions of accurate multipole codes HYDROMULTIPOLE [63], which also include lubrication effects close to the wall, even for distances when the length of the rod and the wall-rod distance become comparable, provided that no point of the rod comes close to touching the boundary.

In Article **[A1]**, we employed the analytical expressions evaluated within the approximation described in **[A9]** to investigate the dynamics of approach of rod-shaped nanoparticles to a nanopore. The paper was co-authored by my PhD student, Radost Waszkiewicz, and was chosen to be part of paper series *Emerging Leaders 2020* in Physics of Fluids.

Nanopore sequencing is now an established technique used to determine the structure of biomacromolecules [64, 65], including DNA [66], RNA [67], and proteins [68]. These biomolecules are typically slender filaments, which are electrophoretically attracted to the nanopore and then translocated through an orifice. The passage through a nanopore is controlled by an interplay of electrostatic [69, 70], electrokinetic [71], entropic [72], osmotic [73, 74] and mechanical forces [75], is now well understood and explored. Much less is known about the approach to the pore. Existing models introduce a minimalistic description of the nanoparticle by a single diffusion coefficient D and an electrophoretic mobility. In this way, the Smoluchowski equation formalism [11] may be used to determine the concentration profile of DNA near the pore [76], and the determination of the range of interaction, called the capture radius [77], being the distance at which the energy of thermal fluctuations become comparable to the electrostatic potential energy. This notion was later extended to the orientational capture radius [78], being the range at which the electric field strongly orients rod-like particles. In all these models, the effects of anisotropy of the particles are neglected, and hydrodynamic interactions with the wall, which hinder diffusion at close distances, are not accounted for. Since hydrodynamic effects are known to alter the trajectories of close sedimenting particles [54, 55] lead to a general slow-down of colloidal dynamics [79], the assessment of their influence is an important research question. Our contribution **[A1]** is a step in this direction. The nanopore is modelled as a point charge which attracts a uniformly charged rod-like particle. We focus on particles which can be modelled as stiff rods. This is appropriate for objects of length L shorter than their persistence length L_p. Examples of such nano-rods are dsDNA fragments shorter than $L_p \approx 50$ nm (or ca. $150bp$) or fd-viruses [80], with $L = 880$ nm and $L_p = 2.8$ μm, translocating through solid-state pores [81]. For longer filaments, the effects of elasticity and ease of conformational change can lead to coiling [82] or even knotting [75, 83] and must be accounted for in modelling. Within our model, we formulate a detailed theoretical approach which accounts for anisotropic diffusivity of a rod-like particle in a viscous fluid. The anisotropy comes from both its non-isotropic shape and the particle-wall interactions. The model was used firstly to determine the time scales corresponding to the different dominant driving mechanisms of the motion: purely Brownian motion far away from the attractive pore, translation and rotational reorientation due to the electric field of the pore, and the wall influence region at close distances to the boundary. We demonstrated that far away from the pore, the motion of the particle is purely Brownian, but as soon as it reaches the electrostatic capture radius, it is systematically attracted towards the pore. Its initial dynamics are then governed by an electrostatic force driving its translational motion, with the velocity resulting from a balance between electrostatic forces and the fluid drag force. Since the latter depends on the orientation of the particle, the motion resembles sideways gliding towards the pore. At closer distances, the electrostatic torque becomes pronounced and strongly aligns the rods with the electric field lines. These allow us to determine a phase diagram showing different regions of dominant interactions in Fig. 3(middle).

After establishing the scaling arguments, we provide a quantitative insight into the dynamics by solving the equations of motion numerically for a collection of initial positions and orientations at intermediate distances, when Brownian motion can be neglected, but the rod is far enough from the pore to disregard the field and flow effects of the pore geometry. We employed an approximate analytical scheme derived in **[A9]** and presented in Eqs. (10), in which the friction tensor of a colloid close to the wall can be decomposed into its bulk value, encoding the particle anisotropy, and a wall-induced correction. This allowed us to formulate a deterministic system of equations which can be solved for arbitrary initial position and orientation of the nanorod. The generated data are used to assess the range of initial conditions for which the effect of the wall qualitatively changes the approach dynamics. For starting points at a large polar angle, measured from the wall to the rod-pore direction, we find that gliding trajectories are governed by the shape anisotropy of the rod, and the wall plays no significant role. However, for smaller angles of approach, hydrodynamic interactions with the wall

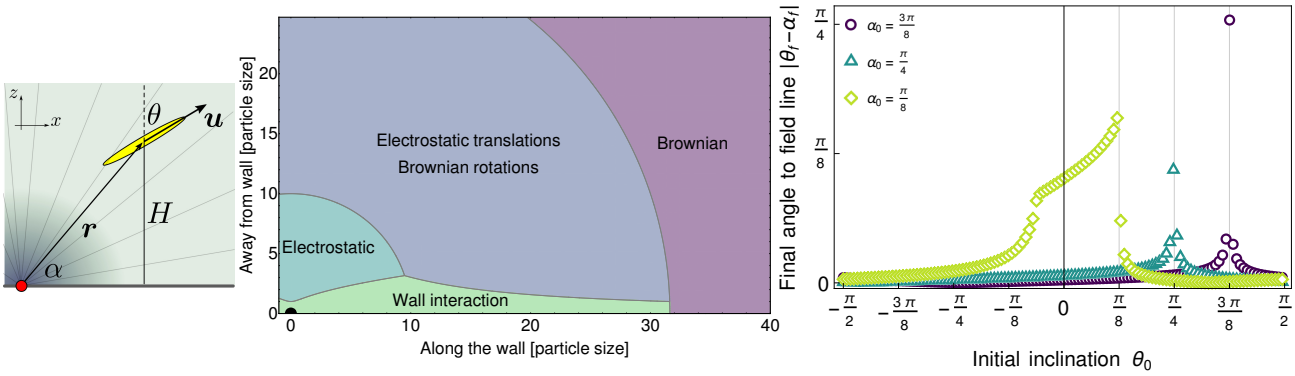

Figure 3: *(Left)* Sketch of a nanorod close to a nanopore (denoted by a red dot). The pore produces a radial electric field, modelled by a point charge at the origin. The configuration of the rod is given by its position $\boldsymbol{r}$ and orientation $\boldsymbol{u}$, which corresponds to an inclination angle θ. In addition, we denote by α the polar angle at which the rod is seen from the pore. *(Middle)* The division of space into regions colored by dominant terms determining the dynamics of the nanorod. The pore is located at the origin, and the wall coincides with the bottom border of the graph. Closest to the surface, wall interaction terms are the most important. Further away from the wall, we anticipate regions of (i) electrostatically determined dynamics, (ii) electrostatic translations with Brownian rotations, and (iii) fully Brownian dynamics. This reflects the fact that electrostatic torque decays faster with the distance from the pore than the force. The boundaries between subsequent regions are obtained by comparing the respective times scales of motion. *(Right)* The angle between the rod and the electric field line close to the pore versus against the initial inclination angle for different starting positions far away from the pore with different polar angles: $\alpha_0 = \pi/8$ – close to the wall, intermediate $\alpha_0 = \pi/4$, $\alpha_0 = 3\pi/8$ – far away from the wall. Trajectories with $\theta_0 < \alpha_0$ are convex and initially glide towards the wall, and trajectories with $\theta_0 > \alpha_0$ are concave and initially glide away from the wall. For small α_0 this relationship is asymmetric due to wall influence where the hydrodynamic torque from wall drag competes with electrostatic reorientation in the late stages of movement. Reprinted from **[A1]**.

significantly alter the angle at which the rod approaches the near-pore region. In Fig. 3(right) this corresponds to the asymmetry of the angle the rod makes with the radial electric field lines as it approaches the pore, starting from different initial inclinations. We have found the extent of this region to be as large as $\pi/8$ which accounts for nearly 40% of spherical area in 3D, thus signifying the importance of wall effects in the proper modelling of dynamics in confined geometry.

Our work shows, basing on the derived scalings, that the neglect of Brownian motion in the near-pore region is justified. Previous works on a similar system included Brownian motion on the level of translational motion only [78]. However, in order to properly resolve the question of Brownian displacements and rotations, both the non-spherical shape of the rod and the presence of the wall should be included. This leads to an anisotropic bulk diffusion (translational and rotational), distance-dependent hindrance of motion, and translation-rotation coupling. Even then, we would expect the effect of Brownian motion to be pronounced outside the near-pore region which is dominated by electrostatic interactions. Including these effects would be an interesting direction of future research.

Elastohydrodynamic effects in confinement

Hydrodynamic interactions between microparticles and organic membranes play an important role in many medical and biological applications. Important examples include drug delivery and targeting using nanocarriers [84–86] which release active agents at tumours or inflammation sites. In navigation through the cardiovascular systems, or during endocytosis [87–89], nanoparticles can come close to membranes of cells or veins which

alter their hydrodynamic mobilities. Over the last few decades, considerable research effort has been devoted to study the motion of particles in the vicinity of interfaces.

The now classical example of the influence of hydrodynamic interactions is a solid spherical particle near a rigid no-slip wall which has been studied theoretically in detail [29, 30, 32, 90], but theoretical predictions have been developed also for a sphere at an interface separating two immiscible liquids [33, 35, 91–96], an interface with partial-slip [37, 39] and a membrane endowed surface elasticity [97–105]. Elastic membranes differ from both liquid-solid and liquid-liquid interfaces as the elasticity of the membrane introduces a memory effect in the system causing, e.g., anomalous diffusion [102] or a sign reversal of two-particle hydrodynamic interactions [104]. On the experimental side, near-wall mobility of a spherical particle has been investigated using a range of optical techniques, involving optical tweezers [106–109], digital video microscopy [110–112] and evanescent wave dynamic light scattering mentioned before. The influence of a nearby elastic cell membrane has been further investigated using optical traps [100, 113–115] and magnetic particle actuation [116]. Particles with a non-spherical shape such as spheroids or rod-like colloids have also received considerable attention. The first attempt to investigate the Brownian motion of an anisotropic particle dates back to Perrin [117, 118] who computed the drag coefficients for a spheroid diffusing in a bulk fluid. A few decades later, Batchelor [119] pioneered the slender-body theory, further developed later [120, 121]. The method has successfully been applied to a wide range of external flows [122] and near boundaries such as a plane hard wall [123–125] or a fluid-fluid interface [126].

From an experimental standpoint, diffusion measurements are available e.g. from video-microscopy of micrometer-sized ellipsoidal particles [127–129]. Experiments with actin filaments were also conducted using fluorescence imaging and particle tracking [130], finding that the measured diffusion coefficients can be accounted for by a correction based on the hydrodynamic theory of a long cylinder confined between two walls. Rotational diffusion coefficients of confined carbon nanotubes have been measured using fluorescence video microscopy [131] and optical microscopy [132]. More recently, the three-dimensional rotational diffusion of nanorods [133] and rod-like colloids have been measured using video [134] and confocal microscopy [135]. Yet, the motion of a spheroidal particles in the vicinity of deformable elastic interfaces has received limited attention.

In Article **[A8]**, we provide an insight into the dynamics of rod-like particles close to a planar elastic membrane. The paper is co-authored with A. Daddi-Moussa–Ider and S. Gekle. It builds on the central result of Ref. **[A9]** being the leading-order mobility corrections of an arbitrary axisymmetric particle near a hard wall. The result presented there can be expressed in closed form by combining the appropriate Green's function with the particle's bulk mobility. For the elastic membrane, we use the Skalak model [136], which is a popular choice to represent red blood cells membranes [137–140]. The elastic properties of the interface are characterized by two parameters – the elastic shear modulus κ_{S} and the area dilatation modulus κ_{A}. Resistance against bending has been included following the model of Helfrich [141] with the associated bending modulus κ_{B}. In this approach, the linearized tangential and normal stress jumps across the membrane are related to the membrane displacement field $\boldsymbol{h}$ and the dilatation ϵ. In the case of periodic forcing or time-dependent deformation of the membrane, the quantity of interest is the frequency-dependent mobility tensor. In confined geometry, due to the presence of the interface, the near-membrane mobility tensor will then have a correction on top of the bulk mobility $\boldsymbol{\mu}_0$, which takes the form $\boldsymbol{\mu}(\omega) = \boldsymbol{\mu}_0 + \boldsymbol{\Delta\mu}(\omega)$, with the second term coming from the interaction of the flow induced by the particle with the boundary. To determine the approximate form of $\boldsymbol{\mu}(\omega)$, we use the results of **[A9]** and generalize them to the case of an elastic membrane. The same methodology can be applied to the case of a membrane, provided that the form of the Green's tensor for the system, $\boldsymbol{G}$, is known. To this end, we first write out expressions, derived in **[A9]**, for the near-wall friction tensor which takes the form $\boldsymbol{\zeta} = \boldsymbol{\zeta}_0 + \boldsymbol{\Delta\zeta}$, as in Eq. (9), with $\boldsymbol{\zeta}_0$ being the bulk friction tensor of an axisymmetric particle. Next, using the relationships between the elements of the grand mobility tensor, we invert them and expand to obtain a leading-order approximation to the mobility correction $\boldsymbol{\Delta\mu}$. These expressions, apart from a power-law behaviour in appropriate powers of the inverse particle-wall distance, as presented in Eq. (10), contain elements of the bulk

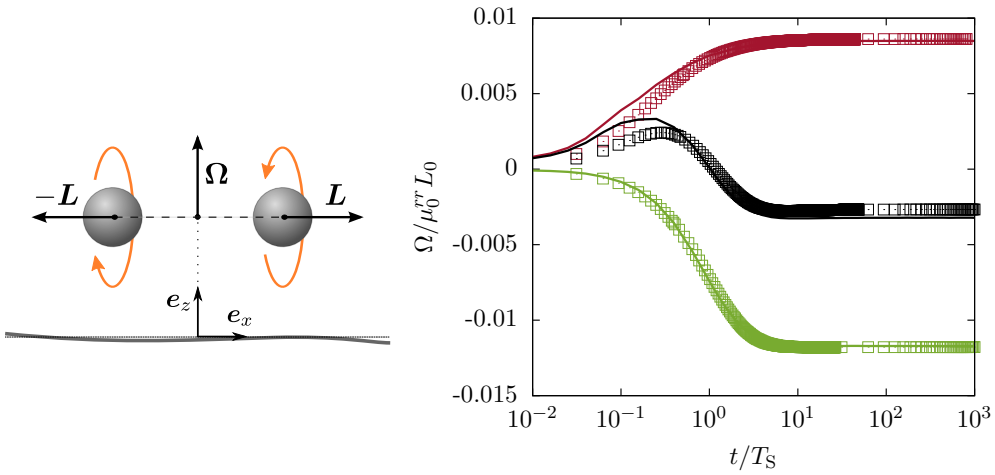

Figure 4: *(Left)* Illustration of two spheres in a torque-free dimer. Torques $\boldsymbol{L}$ of the same magnitude and opposite directions about the centerline are applied to the particles. The membrane-induced rotation-translation coupling leads to a collective rotation about membrane-normal direction with an angular velocity $\boldsymbol{\Omega}$. The doublet remains parallel at the same height above the membrane. *(Right)* Scaled rotation rate of the doublet versus the scaled time near a membrane of pure shearing (green), pure bending (red) and both shearing and bending rigidities (black). Analytical predictions derived in the paper **[A4]** are drawn in solid lines and symbols refer to boundary integral simulations. The time scale of the induced rotation of the pair is considerably slower than that related to the internal rotation of each sphere under the applied torque. Figures reproduced from **[A4]**.

mobility tensor and directional tensors depending only on the orientation of the particle. The directional tensors are found as appropriate directional derivatives of the near-membrane Green's function. The Green's tensor was derived earlier in Ref. [103]. In **[A8]**, we compute these directional tensors explicitly and thus we are able to write down explicit expressions for the frequency-dependent elements of the near-membrane mobility of an arbitrary axisymmetric particle. In the paper, we also list explicit expressions for an ellipsoidal particle for all types of motion: translation, rotation and coupling terms. The mobility corrections are frequency-dependent complex quantities due to the memory induced by the membrane. They are expressed in terms of the particle orientation and two dimensionless parameters that account for the shearing- and bending-related contributions. In the zero-frequency limit, or equivalently for infinite elastic and bending moduli, we recover the mobilities near a hard no-slip wall. We apply our general formalism to a prolate spheroid and find very good agreement with boundary integral method (BIM) numerical simulations performed for a truly extended spheroidal particle over the whole frequency spectrum.

Continuing this line of thought in Article **[A4]**, we extend the analysis above to the problem of translation-rotation coupling and rotational hydrodynamic interactions between two spherical particles near a planar elastic membrane that exhibits resistance against shearing and bending, identical to the one described above. The paper is co-authored with A. Daddi-Moussa-Ider, S. Gekle, A. Menzel, and H. Löwen. To study the hydrodynamic interactions between two spherical particles close to a membrane, we use a combination of the multipole expansion and Faxén theorems to express the frequency-dependent hydrodynamic mobility functions as a power series of the ratio of the particle radius to the distance from the membrane for the self-mobilities, and as a power series of the ratio of the radius to the interparticle distance for the pair mobilities. In the quasi-steady limit, corresponding to zero frequency, we find that the shearing- and bending-related contributions to the particle mobilities have either additive or suppressive effects, depending on the membrane properties and on the geometric configuration of the interacting particles relative to the membrane. To explore further the changing sign of the particle self- and pair mobilities, we analyse an example of a torque-free doublet of counter-rotating particles near the elastic membrane, and depicted in Fig. 4. We find that the induced rotation rate of the doublet

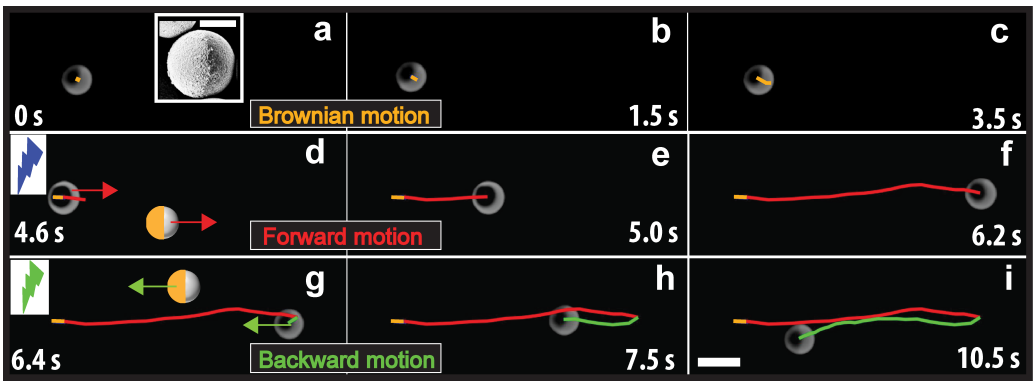

Figure 5: Microscopy images showing the mode of the motion and typical trajectories of the Janus particles described in **[A3]**. The half-Au coated anatase particles are immersed in hydrogen peroxide solution. The bright side is the titania side, while the dark side is the half gold-coated cap. In the schematic, the gold colour corresponds to the gold-coated side of the particle. The colour of lightning-bolt illustrates the wavelength of light used in the experiment. (a-d), Free Brownian motion of the particle. Inset shows a scanning electron microscopy (SEM) image of the Au-coated TiO_2 Janus particle. (e-h), Swimmer propelling in the forward direction under the UV-light illumination. (i-l), Swimming direction of the particle is reversed when we switch to green light. The arrow depicts the direction of motion. Scale bar is 5.0 μm. Scale bar in the inset is 2.0 μm. Figure reproduced from **[A3]**.

around its center of mass depends on the membrane shearing and bending resistance, and an appropriate combination of these parameters can change both the magnitude and the direction of rotation. Near a membrane with shearing resistance only, akin to that of certain elastic capsules, the direction of rotation of the doublet is the same as it would be near a no-slip wall. However, near a membrane which exhibits resistance against bending only, thus resembling a fluid vesicle [142], we observe a reversed rotation direction. The described behaviour can alter the near membrane dynamics and behavior of force- and torque-free flagellated bacteria and swimming microorganisms that use helical propulsion as a locomotion strategy [143, 144]. Our theoretical results obtained in the paper again compare favourably with BIM simulations over the whole range of applied frequencies.

Active transport in confinement

Active systems such as microorganisms and self-propelled particles show a plethora of collective phenomena, including swarming, clustering, and phase separation. In all these, having control over the propulsion direction and switchability of the interactions between the individual self-propelled units may open new possibilities to design materials from within. In Article **[A3]**, together with H. Vutukuri, E. Lauga, and J. Vermant, we present a novel system of self-propelled particles. The Janus particles are made of anatase TiO_2 and are half-coated with gold. Using different wavelengths of illuminating light, we can quickly and on-demand reverse their propulsion direction by exploiting the different photocatalytic activity on both sides. In the paper, we demonstrate that the reversal of the propulsion direction of near-wall ensembles of active particles can drive the particle assemblies to undergo fusion- and fission-like transitions. We also show these active colloids can act as nucleation sites, but also offer to switch rapidly the interactions between active and passive particles, leading to reconfigurable assembly and disassembly. The experimental findings are aptly described by a minimal hydrodynamic model, of which I am the main author.

The design of artificial microswimmers or self-propelled particle systems is currently a subject of vast interest in active matter. Firstly, they are model systems to study the collective behaviour of their more complex natural inspirations. Secondly, they exhibit a variety of non-equilibrium phenomena, such as active clustering,

segregation, and anomalous density fluctuations [145–148]. Several experimental studies have reported on artificial microswimmers using different swimming strategies [145–154]. One class consists of internally-driven phoretic systems of which Janus particles are an important example. Janus particles, named after the two-faced Roman god, possess two sides of different surface characteristics, and induce motion by converting (e.g. chemical) energy on one side of the particle from its local environment [145–148, 155] into their kinetic energy. In these synthetic systems, the only reorientation mechanism is the rotational diffusion of the particle, since the direction of its propulsion velocity vector with respect to the coated hemisphere remains constant [148, 155]. The position and/or the orientation of externally-driven swimmers can be controlled using lab-controlled stimuli such as magnetic, and electric fields [150, 151, 156]. However, in this case field-induced long-range dipole-dipole interactions between the particles by the external fields are unavoidable [157–159], and can preclude studies of collective behavior controlling solely the activity [156]. Only recently, proof-of-principle studies considered a single internally-driven artificial swimmer achieving propulsion direction reversal using a wettability contrast on both sides of Janus particles at different temperatures [152, 160], but being limited by heat transfer rates, these are inherently slow. For studying collective behaviour, one needs the dynamics of switching to be faster than the rotational diffusion timescale of the systems. Importantly, some microorganisms display fast periodic reversals of the direction of motion. Examples include *Myxococcus xanthus* [161], *Pseudoalteromonas haloplanktis* [162], and *Vibrio alginolyticus* [163], but these swimmers use rather complex molecular mechanisms. In consequence, these marine microorganisms show a rich collective behaviour, exemplified by accordion wave patterns [164], and high-performance chemotaxis [165]. Controlling and switching the nature of interactions (*e.g.,* attractive to repulsive, and vice-versa) between individual units without changing the chemistry of starting building blocks is a major challenge in soft condensed matter. Yuan et al. [166] have recently achieved this by exploiting the difference in the elastic response of a complex liquid crystal matrix to light modulation.

In our work, we design synthetic active particles capable of performing fast propulsion direction reversals by simply changing the wavelength of light, from UV to green light. In order to achieve such a model system, we take advantage of the different photocatalytic activity of a single Janus particle. Control over the surface chemistry enables a rapid reversal of propulsion direction, as depicted in Fig. 5. Our system is nearly two-dimensional (2D), which makes it easy to image and ideally suited to address the question of influence of the propulsion direction reversal on the collective behaviour. As an example, we investigate the ability of these active particles to drive the passive particles into dynamic and reversible 2D assemblies via light-switchable propulsion. The photocatalytic decomposition of hydrogen peroxide produces concentration gradients which depend on which side is being activated. As the particles are force-free, the phoretic forces resulting from the concentration imbalance around the particles, need to be compensated by a directed motion subject to fluid drag. However, the heaviness of the gold cap biases the orientation of the cap relative to the wall. As a consequence, the symmetry of the resulting hydrodynamic flow fields of the active particles depend on their orientation. This determines interactions between active and passive particles. In addition, to investigate the effect of cap orientation further, in a separate experiment we use additional external magnetic field to control the cap orientation and show that the interaction between active and passive particles can be switched between attractive to repulsive and vice-versa by changing the cap orientation. Next, we study phoretic flow fields created by active particles attached to a wall with the cap orientation being fixed. These experiments are also used to better understand the flow fields around individual particles.

From the point of view of modelling, we propose a minimal hydrodynamic description. Firstly, we analyse the clustering behaviour observed around active particles in groups. Previous theoretical studies have predicted the hydrodynamically mediated diffusiophoretic attraction and repulsion between the pairs of isotropic particles would lead to clustering and self-propulsion of their assemblies [167]. In our experiments, when a cluster of isotropic TiO_2 particles is exposed to UV illumination, surprisingly, particles start to move outwards radially. The overlaid trajectories reveal the motion of isotropic particles, as shown in Fig. 6a-h (top). In our experiments, we find that the average velocity of the particles versus time shows a power-law dependence $V \propto t^{-0.69}$. We

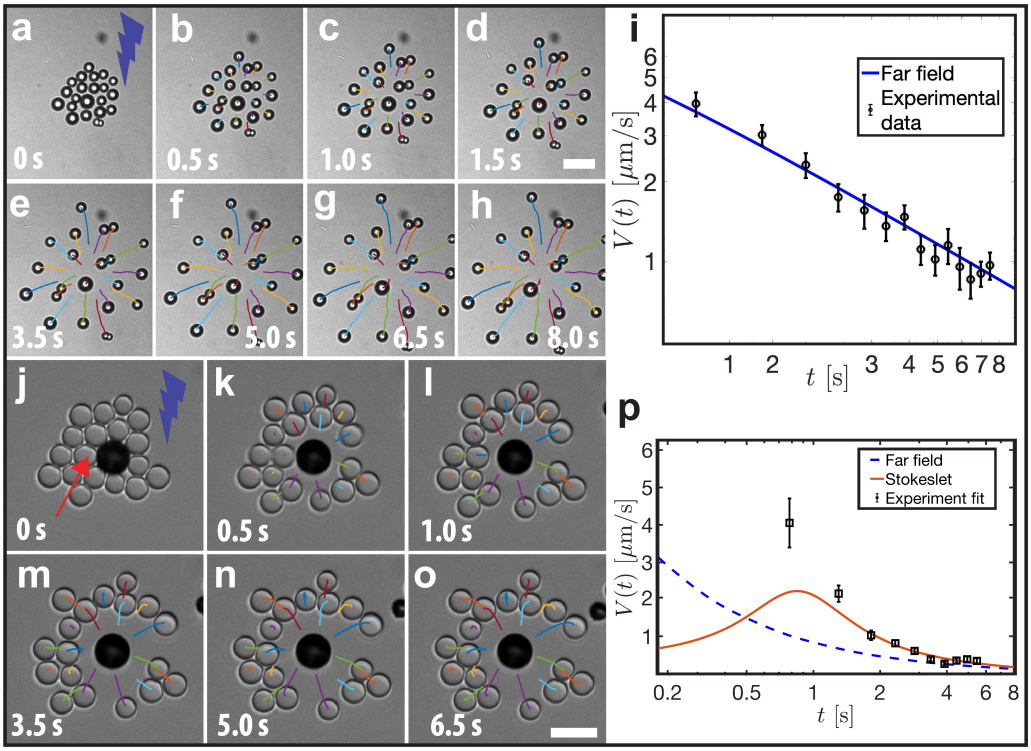

Figure 6: *(Top) (a-i)* Response of the isotropic TiO_2 particles under the illumination of UV-light. (a-h), Photos show the isotropic repulsion behaviour of individual swimmers against neighbouring particles. Overlaid trajectories show the dynamic response of the particles. (i), The average velocity of the particles decays with time as $V \propto t^{-0.69}$ and follows the predicted far-field scaling ($t^{-2/3}$). The blue broken line is prediction of the theoretical model obtained by numerical simulations. *(Bottom) (j-p)* Dynamic response of the passive particles to an immobile active particle under the illumination of UV-light. (j-o), Overlaid trajectories show the passive particles experiencing isotropic repulsions and escaping radially. (p), An empirical fit of the experimental velocity data to the predictions of the theoretical model for the dynamics of tracer particles (solid line). The experimental average velocity over the all particles decays with time and follows the numerically-obtained flow field produced by an immobilized active particle, modelled as a near-wall Stokeslet. Blue line is the far-field prediction which is expected to be valid for much longer times. Scale bar is 5.0 μm. Figure reproduced from **[A3]**.

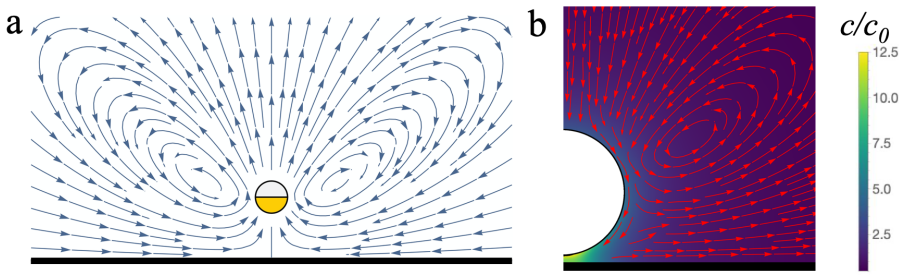

Figure 7: *a) (Left)* Flow streamlines due to a Stokeslet (point force) perpendicular to a no-slip wall. The sucking effect in the plane of the wall dies out with the distance d as $1/d^4$. *b) (Right)* The calculated solute concentration field around an isotropic TiO_2 particle in proximity to a wall, and the corresponding hydrodynamics flow field. Figure reproduced from Supplementary Information to **[A3]**.

explain this behaviour using a scaling argument by modelling the particles as sources of a solute, the gradient of which along the surfaces of the particles gives rise to a phoretic slip [155, 168, 169], which in turn induces flow in its surroundings. In the far field limit, an isotropic sphere produces a chemical concentration field which dies out with distance as r^{-1}. If another sphere is placed at a distance l and is regarded as moving in the concentration field of the first sphere, we find that its leading-order velocity, and finally integrate it to find $V \sim t^{-2/3}$, which is very close to experimental observations. To gain a further insight into the observed dynamics, we performed numerical simulations taking into account pairwise interactions of particles due to their induced phoretic flows. Starting from the initial positions taken from the corresponding experiment, the simulation shows similar trajectories. An empirical fit to the experimental data for the velocity shows good agreement with simulations and the theoretical scaling in Fig. 6i. These experimental findings suggest that the observed repulsive interactions between the Janus particles under UV light can be attributed to a self-diffusiophoretic effect. On the other hand, the Janus nature of the particle greatly amplifies what effectively can be described as a repulsive behaviour. We observe this in an experiment involving a single active Janus particle glued to the surface and surrounded by passive tracers, as depicted in Fig. 6j-o (bottom). The repulsive flow due to a fixed particle can be described in a minimal model by a Stokeslet near a wall [22], depicted in Fig. 7a. In contrast to earlier work involving attraction by an immobilized active particle [170], the dynamics in our case are restricted to a 2D plane parallel to the wall at a distance h. The velocity of a tracer depends on the distance from the Stokeslet as $R/(R^2+4)^{5/2}$, where $R = r/h$ is the rescaled distance [171]. This relation can be integrated numerically to find the velocity of passive tracer particles which can be empirically fitted to the experimental data (Figure 6p). A good agreement with the experimental far-field behaviour of the in-plane Stokeslet flow, decaying as $1/R^4$, is found. In the near field the Stokeslet fails to describe the observed behaviour. This is expected, since other factors come into play (e.g., steric, slip, lubrication, and potentially electric interactions). Furthermore, the change in illumination will only lead to the reversal of the direction of the flow and the magnitude of the Stokeslet, not affecting its qualitative characteristics. In order to fully describe the flow field around a phoretic sphere near a wall, we perform detailed calculations of the concentration and flow field, which may be formulated as the Laplace and biharmonic equations, respectively, and are solved in bi-polar coordinates. The solutions have the form of series representations. Exemplary calculations for phoretic flows in this geometry may be found in [172],**[B8]**. The resulting flow field is depicted in Fig. 7b, showing clear differences from the Stokeslet model.

In summary, in Ref. **[A3]** we propose a route to produce switchable photocatalytic artificial swimmers which exhibit an almost instantaneous reversal of propulsion direction by light modulation. The fast switching makes enables us to direct the assembly and disassembly by the control of the wavelength and intensity of illuminating light. In the presence of many swimmers, we observe growth of active clusters as a consequence of the solute-mediated long-range attractions. A reversal of the propulsion direction leads to the the breakage

of clusters resembling a fission-like process. We are able to qualitatively explain the experimental results using a simple hydrodynamic scaling. We believe that the process of forced disintegration, as opposed to free Brownian spreading, has new dynamical features which allow greater control over the collective dynamics of phoretic active matter. Our system, with fast-switchable interactions from attractive to repulsive and back, paves a new way to design reconfigurable materials by sculpting them from within. Moreover, the presented experimental system opens an avenue for developing a new theoretical framework of active systems where the propulsion velocity can take multiple values and orientations with respect to the particle.

Artificial microswimmers near boundaries

Swimming microorganisms use myriads of different strategies to achieve propulsion or stir the suspending fluid [173–175]. To overcome the constraint of time-reversibility of the Stokes equations governing the small-scale motion of a viscous fluid, known as the famous Purcell's scallop theorem [176], many of them perform a non-reciprocal motion of their bodies. Even for an isolated swimmer hydrodynamic interactions with the environment can gravely affect microbial dynamics [177, 178], leading to surface trapping [179], near-wall circular motion [180], accumulation induced by boundaries [181] and by shear flow [182, 183], or swimmer reorientation [184, 185]. The interaction of many swimmers leads to a rich collective behaviour, including the onset of propagating density waves [186–193], alignment and the formation of lanes [194–197], motility-induced phase separation [198–202] and the emergence of active turbulence [203–209]. Some swimming microbes have evolved to sense, react and respond to external flows. Examples are *N. scintillans* dinoflagellates which display bioluminescence to reduce grazing by flow-generating predators [210] and the ciliates *S. ambiguum* which have developed hydrodynamic communication [211].

The long-range nature of hydrodynamic interactions in geometrical confinement can significantly alter the behaviour of suspended particles or organisms [212]. Interfacial effects are crucial for the design of microfluidic systems [8, 38, 213]; they slow down translational and rotational diffusion of colloidal particles [104, 214–216],**[B11,B12]**, and play an important role in living systems, where walls have been shown to change the trajectories of swimming *E. coli* bacteria [179, 217–221] and microalgae [222, 223]. Even the simplest theoretical models of bacterial motion have revealed that the dynamics of a swimmer can be surprisingly rich [224]. It has been demonstrated that geometric confinement can conveniently be utilized to steer active colloids along arbitrary trajectories [225]. A theoretical analysis of detention times of microswimmers trapped at solid surfaces has pointed at the interplay of hydrodynamic interactions and rotational noise driving the attachment process [226]. Trapping in more complex geometries has been explored in the context of collisions of swimming microbes with large obstacles [227, 228] and scattering on colloidal particles [229]. The generic underlying mechanism is thought to play a role in important biological processes, such as the formation of biofilms [230, 231].

The diverse phase behavior has also been confirmed in artificial systems of chemically powered diffusiophoretic particles [232–239], leading to a phase diagram also includes trapping, escape, and a steady hovering state. Swimming near a boundary has been addressed using a two-dimensional singularity model combined with a complex variable approach [240], resistive-force theory [241], and a hydrodynamic singularity representation [144]. A number of other artificial designs have been proposed to construct and fabricate model swimmers capable of self-propulsion in a viscous fluid by internal non-reciprocal actuation. A prominent class among those are simple systems with only a few degrees of freedom necessary to break kinematic reversibility, as opposed to continuous irreversible deformations or chemically-powered locomotion [174, 175, 242–245]. A famous example of such a design is the Najafi-Golestanian swimmer [246] encompassing three aligned spheres; their distances vary in time periodically but with phase differences. This gait leads to locomotion along straight trajectories [247–250]. Importantly, this system has been also realized experimentally using optical tweezers [251, 252]. Following theoretical works, a number of similar designs have been proposed: a system involving one passive and one elastic arm [253, 254], both arms being muscle-like [255] or using a swimmer model made

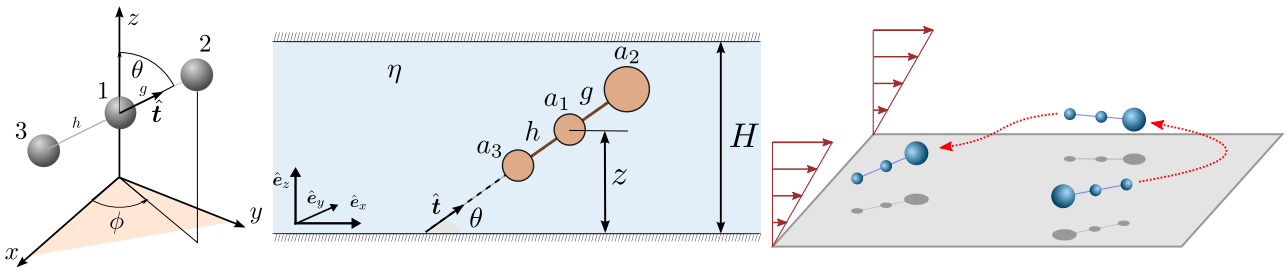

Figure 8: Sketches of the three-sphere swimmer in various geometries. *(Left)* A neutral three linked spheres microswimmer close to a planar no-slip wall. The swimmer is oriented along the unit vector $\hat{\boldsymbol{t}}$ defined by the azimuthal angle ϕ and polar angle θ. The spheres are connected to each other by dragless rods where the instantaneous distances between the spheres 2 and 3 relative to the sphere 1 are denoted g and h, respectively. Reproduced from **[A6]**. *(Middle)* The three-sphere swimmer confined between two planar parallel walls, representing a microchannel. The sizes a_i of the spheres define the swimming characteristics of the microrobot (pusher, puller, or neutral). Reproduced from **[A5]**. *(Right)* A sketch of the 3-sphere swimmer exposed to an external shear flow shows the rheotactic response, leading eventually to an upstream orientation. The swimming characteristics in the presence of an external shear flow are described in Ref. **[A2]**.

of beads and springs [256–258]. An extension of this idea to rotational motion has also been proposed: a circle swimmer composed of three spheres joined by two links at an angle to each other [259], linked like spokes of a wheel [260], or forming an equilateral triangle [261]. A generalisation to a collection of $N > 3$ spheres has also been analysed [262]. Further investigations explored the effect of fluid viscoelastic properties [263–269], swimming motion close to a fluid interface [270–272] or inside a channel [273–277], and the hydrodynamic interactions between a pair of neighboring microswimmers near a wall [278]. These simple models thus exhibit myriads of inherently non-equilibrium dynamic phenomena. Boundaries have also been shown to induce order in collective flows of bacterial suspensions [279–281], promising potential applications in autonomous microfluidic systems [282]. A step towards understanding these collective phenomena is to explore the dynamics of a single model swimmer interacting with a boundary.

In the Articles **[A2, A5, A6]** we focus our attention on the dynamics of a Najafi-Golestanian three-sphere swimmer in the presence of a confining boundary. We focus on the characterisation and classification of the observed behaviour of the swimmer in confined geometry. Schematic representations of the systems considered within this series of papers are depicted in Fig. 8. We will describe them in detail in the following. In **[A6]**, we describe the motion of the microswimmer near a planar hard boundary. In **[A5]**, we perform a similar analysis in the case when the swimmer is confined in a microchannel composed of two parallel, planar walls. In both cases, we observe different behaviour patterns, depending on the swimmer parameters and initial position. In **[A2]**, we incorporate the effect of an external shear flow to study the shear-induced reorientation of the swimmer. We see a pronounced rheotactic behaviour, leading to possible upstream motion, in agreement with observations of bacteria in flows [283].

In the first paper of the series **[A6]**, together with A. Daddi-Moussa-Ider, C. Hoell and H. Löwen, we focus on the simple 3-sphere swimmer near a planar hard wall, as sketched in Fig. 8(left). First, we introduce the model for the Stokesian dynamics of the swimmer. In this contribution, we consider a Najafi-Golestanian swimmer composed of three identical spheres, which means that its hydrodynamic flow field has no dipolar contribution – such a swimmer is thus called neutral. The swimmer is immersed in a quiescent fluid, and the forces and velocities of the spheres are linearly related. We also impose the constraint of a rigid-body motion of the swimmer. Since in microscale swimming the self-generated propulsion force and torque are balanced by the hydrodynamic drag and torque, respectively, our model imposes this condition to determine the propulsion velocity. The motion is driven by pre-defined oscillations of the distance between subsequent spheres. We also allow for rotations of the spheres about the long axis of the swimmer. These properties allow us to derive

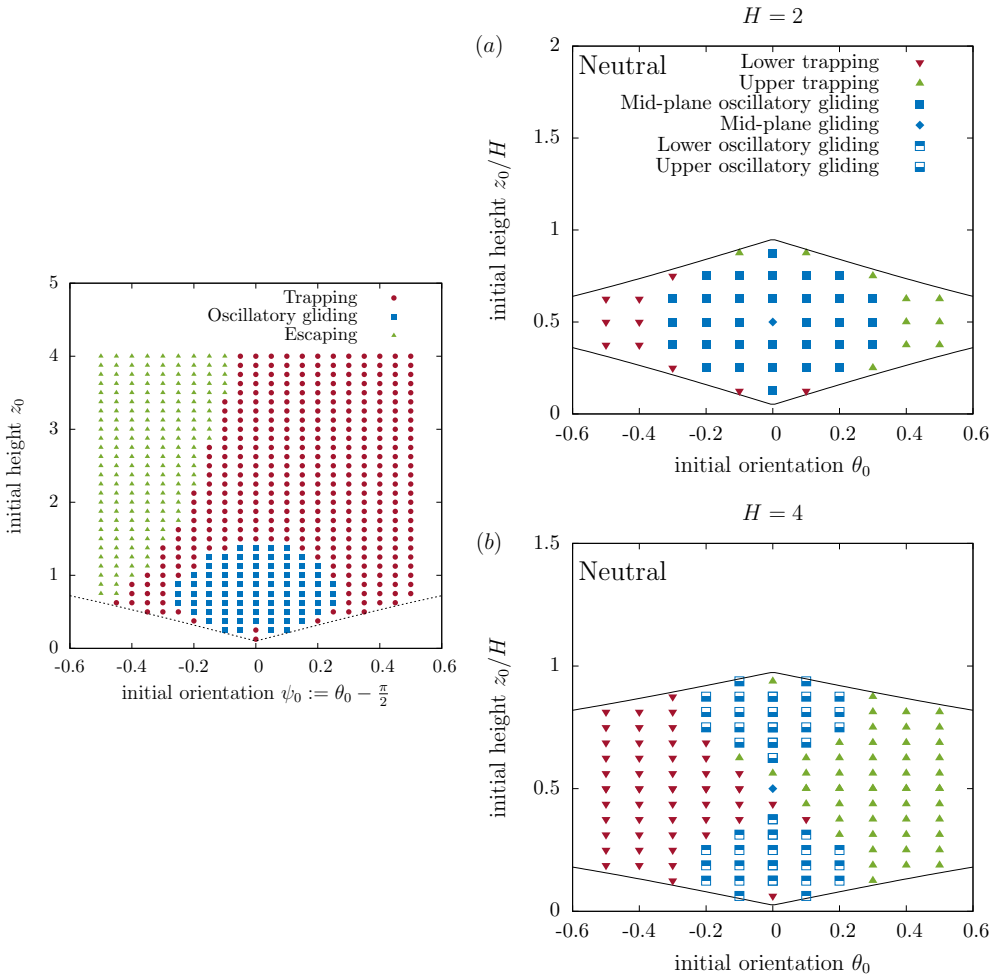

Figure 9: *(Left)* State diagram illustrating the possible swimming scenarios for a three-sphere swimmer near a wall. The dashed line bounds the geometrically accessible region. For this plot, the radii of the spheres are taken to be $a = 0.1L$, with the inter-sphere average distance L. Figure reproduced from **[A6]**. *(Right)* State diagram of swimming scenarios for neutral three-sphere swimmer confined between two parallel walls separated by a distance H for (top) $H/L = 2$ and (bottom) $H/L = 4$. Symbols represent the final swimming states for a given initial orientation and distance along the channel. Solid lines correspond to geometrically excluded situations. We observe states that are similar to those seen close to a single wall, with an additional mid-plane gliding mode. Figure reproduced from **[A5]**.

expressions for the evolution equations for the swimmer, which we integrate numerically to find the trajectories. Hydrodynamic interactions in simulations are calculated in an approximate way using the previously derived expressions for the single-sphere self-mobilities by Cichocki & Jones [284]. For the pair mobility, we use the results of Swan & Brady [30], benefiting from the fact that lower accuracy is needed in this case, as the spheres are rather well-separated by the imposed rigid-body motion constraints.

To characterise the dynamics of the swimmer, we firstly solve the equations of motion numerically to obtain the swimming trajectories. In the case where there is no rotational motion of the individual spheres, the motion remains planar, and we determine the swimming state diagram for a given initial orientation and height of the swimmer above the wall, as shown in Fig. 9(left). Depending on the parameter values, we find three possible scenarios. The swimmer may become trapped by the wall, escape away, or undergo a non-trivial oscillatory gliding motion. In the trapping state, the swimmer approaches the wall and gradually aligns with the wall-normal direction. It then remains hovering at a constant height above the wall. The escaping state is observed for swimmers initially directed away from the wall. The most interesting state, however, is the oscillatory

gliding, where the swimmer exhibits oscillatory motion both raising and lowering the position of its center of mass, and its orientation. Its director follows a similar oscillatory motion. This behaviour is seen only for a region of initial conditions corresponding to low initial height and orientations close to parallel. In order to explore the boundaries between the regions in more detail, we analyse the trajectories at the intersection between different modes of motion, and relate the initial condition to the observed motion characteristics, such as the amplitude and wave length of oscillations. In order to quantify the transitions, we introduce the relevant order parameters in the system.

For the trapping–escaping transition, we choose the inverse of the peak height of the swimmer achieved before trapping, and the inverse distance traveled along the wall corresponding to the peak. We observe that the inverse peak height exhibits a scaling behaviour around the transition to escaping, with an exponent of $1/3$. The inverse peak position also shares this behaviour, although with a different exponent of $5/6$. To study the transition between trapping and oscillatory gliding states, we focus on the average swimming velocity parallel to the wall, scaled by the bulk swimming velocity. As the second order parameter, we choose the oscillation amplitude. Both proposed parameters vanish in the trapping state, as then the swimmer attains a constant height above the wall and aligns with the vertical direction. The transition from oscillatory gliding to trapping is thus first order, with a discontinuity of the order parameter.

To explain this transition behaviour, we developed a far-field model for the dynamics of the swimmer, expressing the relevant mobility functions as a power series in the ratio a/z, with a being the sphere radius and z being the wall-particle distance. Expanding up to the second order in a, and restricting to leading-order terms in $1/z$, we were thus able to derive analytical equations for the averaged dynamics of the swimmer far away from the wall (for the position and orientation). From these equations, we identify the flow field induced by a neutral swimmer near a wall being composed of a combination of two flow singularities: a force quadrupole and a source dipole [122, 144]. This model allows us to find approximate trajectories, which in particular gives us an insight into the behaviour of the order parameters. Indeed, we find analytically that the leading order behaviour of the inverse peak height at the trapping–escaping transition scales with the $1/3$ exponent, and the inverse peak position shows the $5/6$ exponent at transition, which fully explains the numerical predictions of the fully-resolved hydrodynamic model.

In the final part, we incorporate internal rotations of the individual spheres. Adding this degree of freedom renders the dynamics fully three-dimensional. However, upon adjusting the definition of the order parameters in this case, and the corresponding far-field model which maps again onto a quasi-2D dynamics, we recover the same scalings as described before. Thus we confirm that according for the dominant flow field is sufficient to recover the general features of the dynamics of a three-sphere swimmer near a wall. Interestingly, recent experimental realizations of such a swimmer using optical tweezers [251, 252] open the possibility of verification of the proposed description in laboratory conditions.

Pursuing the method of analysis proposed in Ref. **[A6]**, we have applied a similar modelling strategy to the problem of motion of a three-sphere swimmer in a channel. To this end, in Ref. **[A5]**, written in a broad collaboration with A. Daddi-Moussa-Ider, A. Mathijssen, C. Hoell, S. Goh, J. Bławzdziewicz, A. Menzel, and H. Löwen, we analyse the motion of a model swimmer enclosed between two planar and parallel no-slip walls, as sketched in Fig. 8(middle). The channel height H is now another parameter influencing the dynamics. In this study, differently to **[A6]**, we extend our analysis from neutral to pusher- and puller-type swimmers. The far field characteristic flows of the latter two have a dipolar character, which corresponds to a longer range of interaction than that of a neutral swimmer. This is achieved by allowing different radii of the constituent spheres. The kinematics of swimming are imposed identically to Ref. **[A6]**, and the main difference is encoded in the hydrodynamic effect of the confining walls. The Green's function for a channel created by two parallel planar walls was first derived by Liron and Mochon [285] by combining Fourier transforms with the image method. Alternatively, following the method of Mathijssen *et al.* [41], the Green's function may be expressed as an infinite series of image reflections. However, we adopted a different approach based on the decomposition of

the Fourier-transformed vector fields into components longitudinal, transverse, and normal to the walls. Upon inversion, the Green's functions are then expressed in terms of Bessel integrals of the first kind, and the series can be truncated at a desired order. Here, we allow no internal rotation of the spheres, so the motion again reduces to planar dynamics. We approximate hydrodynamic interactions by restricting to including only self- and pair mobilities of the spheres. For the representation of the hydrodynamic mobility of spheres between two parallel walls, we calculate the self-mobility functions by evaluating the boundary-induced corrections to the flow field at the position of the particle using the method of reflections [7, 12]. We also verify the accuracy of the approximation by comparing with exact multipole method results for two parallel walls [286–288]. We evaluate the pair mobilities from the analysis of the reflection series presented in the paper. The predictions of the full hydrodynamic model allow us again to map the phase space and identify different near-wall behaviour. For a neutral swimmer, exemplary results are plotted in Fig. 9(right). Depending on the channel height, we find areas of different behaviour, but most generally we can distinguish symmetrically placed trapping and oscillatory gliding states close to either the top or bottom wall, as seen before in **[A6]**, and a new state of mid-plane gliding. The onset of the oscillatory behavior observed in neutral swimmers can be attributed to the hydrodynamic quadrupole moment which rotates the swimmer away from the nearest wall [289]. Similar persistent oscillations have also been observed for a neutral squirmer in a capillary tube [274]. The situation becomes different for pushers and pullers. The dominant component of the flow field is now dipolar, and not quadrupolar (as for a neutral swimmer). For pushers, with the front sphere being larger, any oscillations are amplified and no gliding state is present. Eventually all trajectories lead to trapped states at one of the boundaries. For pullers, with a larger aft sphere, we see a different dynamics, in which initial oscillations are eventually damped and the swimmer exhibits a strictly horizontal gliding motion near either the upper or bottom wall. Trapped states are also present, however, for large values of the dipolar coefficient, those are replaced by new sliding states, in which the swimmer maintains a constant non-zero orientation and translates along the channel walls at a constant height. We also investigated analytically the stability of swimming along the centerline by considering perturbations around the symmetric state. We find that above a critical channel width, a pitchfork bifurcation to oscillatory motion appears, and we characterise it analytically. Our findings may be useful for the design of swimming microrobots in confined geometries. The characterisation of the final dynamical states for given initial conditions might be particularly useful for designing microfluidic devices dedicated to microswimmer manipulation and sorting. We have shown that analytical approximations can be profitably used to describe the motion of a model microswimmer.

Both articles described above consider the influence of confining boundaries on the motion of microrobots in a quiescent fluid. However, as mentioned in the introductory part, in many experimentally relevant situations microscopic swimmers are exposed to an external flow. In Article **[A2]**, we focus on the problem of cargo transport by a simple Najafi-Golestanian swimmer [246, 290], in the presence of an external shear flow close to a planar no-slip wall. We consider one sphere to be larger than the others to hold the payload. Depending on whether this is the front or the aft sphere, the swimmer type is a pusher or a puller. The far-field hydrodynamic flow signature generated by such a pusher (puller) corresponds to an extensile (contractile) Stokes dipole [291, 292]. We consider the dynamics of the swimmer subject to an external shear flow. For a swimmer of length $2L$ and a free swimming velocity V_0 (in the absence of walls), the shear flow can be characterised by a dimensionless shear rate $\dot{\gamma}$ such that the dimensional shear rate is $\dot{\gamma}^* = \dot{\gamma}V_0/L$. We determine the swimming dynamics by solving for the hydrodynamic interactions between the spheres and the wall, including the external shear flow, in the Rotne-Prager-Yamakawa approximation, which accounts for the different radii of the particles [17]. Using the shear disturbance tensor formalism, we incorporate the effect of external flow into the dynamics. With these components, we construct the generalised mobility tensor that relates the translational and rotational velocities of each sphere to the hydrodynamic forces and torques. Similarly as before, the motion is determined by enforcing the net torque and force to vanish and by prescribing the oscillatory internal kinetics. We first explore the motion under flow for swimmers starting with arbitrary orientations. Depend-

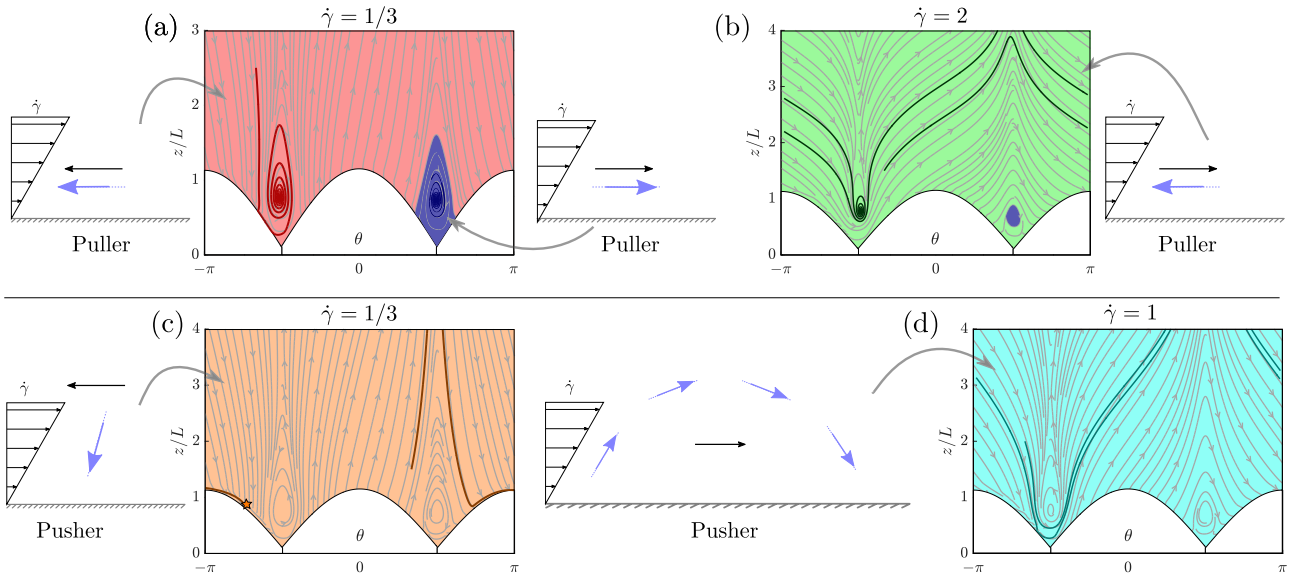

Figure 10: Phase-space diagrams of upstream swimming, showing the dynamics in the height- orientation space for various flow strengths. Grey lines show streamlines in the phase space, while coloured lines mark exemplary trajectories. Background colours indicate the final state. Insets show the corresponding final-state behaviour, with blue arrows on the axis being the director, and the black arrows above showing the net (lab frame) direction of motion, the sum of advection and self-propulsion. *(a)*. Pullers at $\dot\gamma = 1/3$. In the red field, the swimmer ends up swimming upstream, oriented along to the surface. Blue field corresponds to downstream parallel motion. *(b)*. Pullers at $\dot\gamma = 2$. Green field marks downstream motion with upstream parallel orientation. *(c)*. Pushers at $\dot\gamma = 1/3$. Brown field shows all swimmers moving upstream, oriented almost perpendicular to the surface. The orange star indicates the final fixed point. *(d)*. Pushers at $\dot\gamma = 1$. Cyan field marks all swimmers being advected downstream, following an indefinite tumbling motion, detached from the surface. The white arc-like regions are geometrically inaccessible. Figure reproduced from **[A2]**.

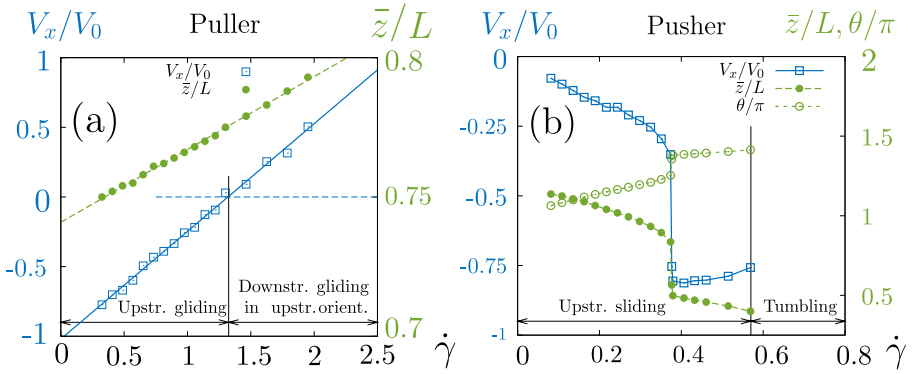

Figure 11: Rheotactic performance of *(a)* pullers and *(b)* pushers, as a function of the applied shear rate. The swimmer velocity $V_x(\dot\gamma)$ is shown in blue squares, with negative values indicating upstream motion, the orientational angle $\theta(\dot\gamma)$ in green open circles, and the position of the central sphere $\bar z(\dot\gamma)$ in green filled circles. Figure reproduced from **[A2]**.

ing on the swimmer type (cargo pusher or puller), we find different reorientation mechanisms, however, all of those lead to a positive rheotactic response, eventually aligning with the flow and swimming upstream. At very strong shear, the swimming speed no longer exceeds the local flow, and swimmers are advected downstream but they can still retain their upstream orientation. Over time, all trajectories thus converge to a two-dimensional shear plane. Both pullers and pushers swim upstream at weak flows, but they do so in a completely different fashion. The three-sphere pullers tend to swim almost parallel to the wall with the director slightly pointing towards the surface. The larger back sphere tends to stick out into the stronger flow, so the puller can rotate against the flow. This reorientation mechanism has been called the 'weather vane effect' [293, 294]. Importantly, the pullers align with the shear plane rather slowly. Pushers, on the other hand, tend to swim almost perpendicular to the surface, with the director pointing slightly upstream. Since the back sphere sticks out into the flow, it gets quickly advected downstream and the swimmer orients upstream. Because the tail sticks out much further in this case, pushers have a much faster reorientation rate due to the stronger 'weather vane effect'. Their cargo can therefore be exploited for enhanced rheotactic response. This fundamental geometric difference also affects the velocity at which the two swimmer types can move against the flow. In the plane of motion along the shear flow direction, we can quantify the swimmer dynamics in the phase space spanned by the wall-separation distance and the director orientation, which become the natural variables for a dynamical system we examine. We classify the rheotactic states by performing the fixed points analysis. Figure 10 shows the evolution of these dynamics in the phase space, with the top row showing pullers and the bottom row showing pushers. The steady-state swimming behaviour correspond to stable fixed points which, however, depend on flow rates. At weak flows, the pullers mostly tend to swim upstream parallel to the surface, with a small fraction of initial conditions leading to downstream parallel swimming. At strong flows, [Fig. 10(b)], almost all pullers are advected downstream, showing a 'toppling' motion, which is transient, and the final stable state is one with an upstream orientation on the surface. At even stronger flows, pullers are oriented upstream but advected downstream. Pushers show a different dynamics, since both fixed points with parallel orientation are unstable. In result, at low shear pushers tend to align with the wall-normal direction, with a little upstream bias [Fig. 10(c)]. Regardless of the initial conditions, all pushers end in this state, marked with an orange star. As the flow strength is increased, the phase portraits remain unchanged. At even larger flows, at $\dot{\gamma} = 1$, the orange star fixed point also becomes unstable, so the pushers detach from the wall and tumble downstream in arc-like trajectories. In the following analysis, having determined the stable fixed points, we determine the properties of these swimming modes for different shear rates. In particular, we compute the translation velocity along the wall (negative for upstream swimming), the orientational angle and the height of the central sphere, finding very different behaviour for pushers and pullers, as illustrated in Fig. 11. Pushers in weak flows can move upstream swiftly at almost their free swimming speed. At higher shear rates, the velocity increases linearly, finally leading to downstream advection at high shear. The upstream swimming velocity tends to zero around $\dot{\gamma} \approx 1.35$. Surprisingly, for pushers we see the opposite behaviour, with the upstream velocity being close to zero in weak flows, but their alignment for stronger flows leads to an increased upstream locomotion at high shear. We see a sharp transition around $\dot{\gamma} \approx 0.38$, where the vertical position of the swimmer suddenly drops so the upstream swimming speed jumps up. Upon increasing the flow, the velocity stays approximately constant until the pushers detach at around $\dot{\gamma} \approx 0.56$.

In summary, we show that both cargo pushers and pullers tend to swim upstream near surfaces, but in a very different manner. The rheotactic performance can be enhanced by exploiting the cargo and tuning the geometry. Different swimming behaviour of pushers and pullers in shear flows may be optimized for different applications. For example, to transport cargo [295] upstream in fluctuating flows, it may be beneficial to use a puller for its robustness, while in strong but stable flows a pusher-like swimmer can be more practical. In comparison to existing experimental realizations, we note that for autophoretic Janus nanorods, the pullers assume a larger tilt angle compared to pushers and they reorient faster against the flow [296], while we see that the opposite is true for three-sphere swimmers. We conclude that the far-field hydrodynamic signature (dipole moment) might not suffice to assess rheotactic performance. Also spherical catalytic Janus particles were observed to move

upstream near surfaces [297]. A natural extension of our work would be to include effects of chirality, relevant to the dynamics of spermatozoa [298, 299] and bacterial flagella [299]. The torque induced by this chirality can lead to the emergence of new dynamical regimes accessible upon crossing threshold critical shear rates [294]. Nevertheless, our work provides important insights into the design strategies aimed at inducing and maximising rheotactic performance.

Two-dimensional wall-bounded diffusion

In the paper **[A7]** we turn our attention to yet another feature of Brownian motion in confinement, namely its reduced dimensionality which may play an important role in the development of theoretical tools for the analysis of experimental data. The paper, co-authored by L. Koens and E. Lauga, was motivated by experiments involving the two-dimensional passive diffusion of boomerang-shaped colloids tracked with video microscopy by Chakrabarty *et al.* [300]. The experimental procedure relies on tracking the geometric centre of the boomerang (CoB), and the measured probability distributions for the position of this point at various times show striking non-Gaussian tails in their probability distribution function. Hence using these data for the characterisation of motion we might encounter anomalous diffusion, including mean drift. In the paper **[A7]**, we develop a general theoretical explanation for these measurements. Our idea relies on calculating the two-dimensional probability densities at the centre of mobility of the particle (CoM), where all distributions are Gaussian, and then transforming them to a different reference point. Our model clearly captures the experimental results, without any fitting parameters, and demonstrates that the one-dimensional probability distributions may also exhibit strongly non-Gaussian tops. These results indicate that the choice of tracking point can cause a considerable departure from Gaussian statistics, potentially causing some common modelling techniques to fail.

Historically, Brownian motion of spherical particles has been characterised both theoretically [301–303] and experimentally [304], thereby relating the internal micro-structure of a fluid to its macroscopic transport properties. This line of thought was then expanded to more complex systems and behaviour, such as diffusing colloids with non-spherical shapes [305, 306] or the ballistic behaviour of a particle shortly after agitation [307]. Only relatively recently have experiments managed to probe these non-spherical [308–311] and ballistic regimes [312]. The ability to probe anisotropic shapes has in turn revealed exciting new behaviours [300, 313], prompting new theoretical models to explain them [314–316].

For an arbitrarily shaped three-dimensional particle moving in a Stokes flow, there exists a special point, called the centre of mobility (CoM), at which the translation-rotation coupling mobility tensors are symmetric [306]. This point can be found explicitly, given the mobility matrix at any point of the particle, using the transformation rules given explicitly in Ref. [317]. At the CoM, the full probability density functions (PDFs) remain Gaussian at all times, in agreement with the classical arguments of Brownian motion [315]. In contrast, off this point the PDFs are not guaranteed to have the same statistics, with both the mean and mean-squared displacement demonstrating transient behaviour not found at the CoM [308, 313, 315, 318]. These transient effects decay with the rotational time scales of the system, and the long-time limit diffusion rates are not only independent of position but also identical to those obtained at the CoM [318].

In a 2D system, the particle has only one rotational degree of freedom, and the centre of mobility (or its two-dimensional analogue, the centre of hydrodynamics CoH) can be defined as the point where the translation-rotation coupling tensors vanish and in effect there is no coupling between translations and rotation [311]. The mobility matrix may be calculated in any frame of reference. In two dimensions, the mobility matrix is a 3×3 tensor, including a 2×2 translational part, a single rotational coefficient, and two coefficients coupling the rotational to translational motion. The corresponding diffusion matrix at the CoH can be determined using the standard two-dimensional mobility matrix transformation rules for Stokes flows [317]. Physically, the two-dimensional centre of hydrodynamics plays an identical role to the three-dimensional CoM, in that the full PDFs determined by tracking this point remains Gaussian at all times. Furthermore, other points will, again, not necessarily generate the same statistics.

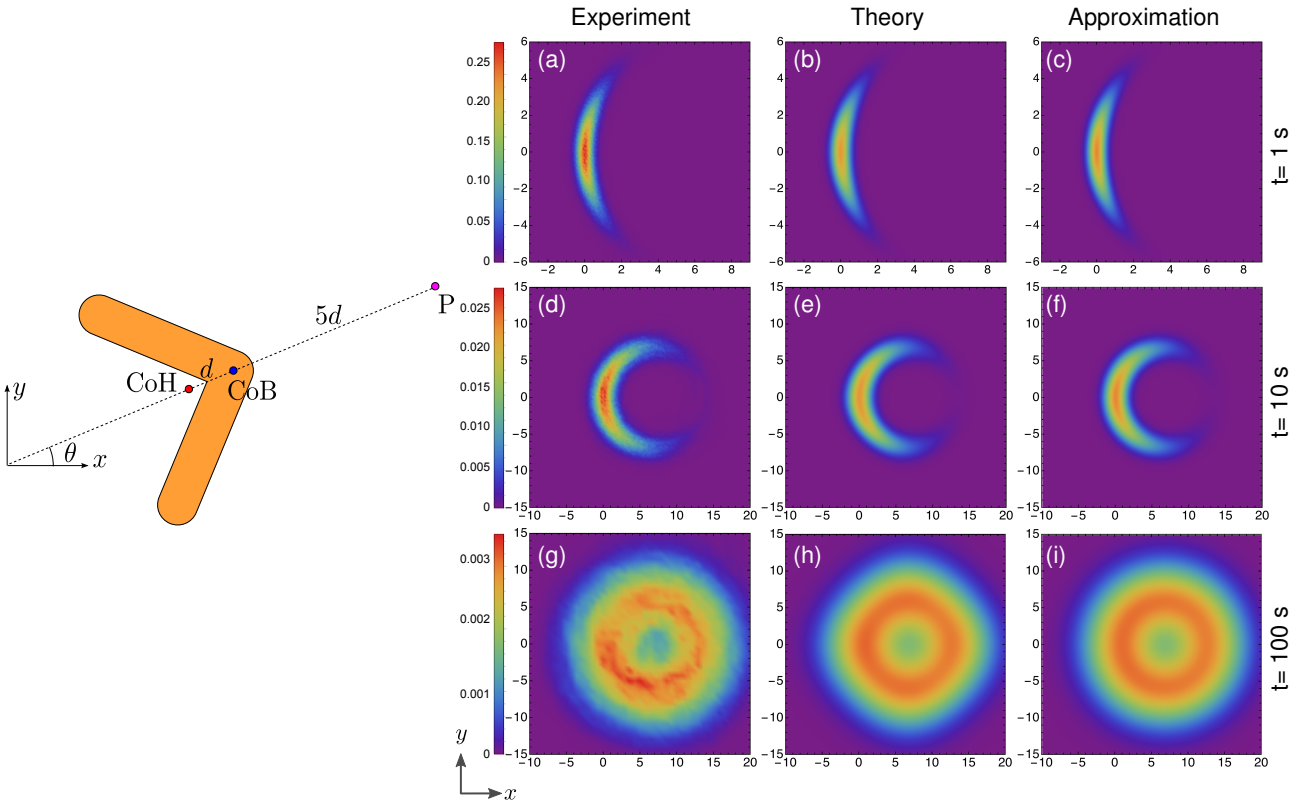

Figure 12: *(Left)* Sketch of the boomerang particle used in the experiments, where we indicate the location of the reference point P, the geometric centre of the body (CoB) and the centre of hydrodynamics (CoM). *(Right)* Two-dimensional probability distribution function, $P(x, y, t)$, at the point P located outside the boomerang. The experimental data (a)(d)(g), originally shown in [300], and provided by the authors to be re-plotted here. The theoretical predictions (b)(e)(h) are obtained by numerical integration of the transformed PDF, while the theoretical approximation (c)(f)(i) are obtained by assuming isotropic drag and expanding the resulting expression in series. Reprinted from **[A7]**.

Ideally, experiments would only track the CoM and the CoH due to the particular simplicity of the theoretical description. However, this is often impractical, as these points can lie outside the body. Therefore, normally measurements track a characteristic physical point of the particle, such as the geometric centre, which may experience transient, and possibly non-Gaussian statistics. In order to characterise these statistics Chakrabarty *et al.* considered the two-dimensional Brownian motion of a boomerang-shaped particle [311, 313]. These shapes are useful as the CoH of these particles lies somewhere between their two arms, and can be displaced by varying the asymmetry in the boomerang arm lengths [311]. In order to determine the position and orientation of the particles, high-precision tracking algorithms have been developed [319]. The works [311, 313] experimentally showed that the mean and mean-squared displacement of a geometric point exhibited a crossover from short-time faster to long-time slower diffusion with the short-time diffusion coefficients dependent on the points used for tracking. This was in turn explained theoretically by solving a set of Langevin equations for the dynamics of the moments. Though these papers fully explained the dynamics of the mean and mean-squared displacement, they did not characterise how non-Gaussian the PDFs at the geometric point were. Chakrabarty *et al.* [300] therefore aimed to characterise the two-dimensional (2D) Brownian motion of a boomerang-like particle when tracked off the CoH and to relate it to the diffusive properties of the particle. They concluded that the PDFs for the geometric centre (CoB, Fig. 12(left)) of the body exhibit strongly non-Gaussian tails when no initial orientation is imposed. These tails are not present when tracking the CoH. Qualitative arguments presented therein related the observations to the previously analysed general concepts of Brownian and non-Gaussian diffusion

[320]. However, the non-Gaussian behaviour was characterised by fitting empirical relations to the measured distributions.

In our paper, we provide a quantitative theoretical description for the PDFs observed by Chakrabarty *et al.* [300]. We first write the explicit expression for the probability density function for the 2D position (x, y) and orientation (θ) of the particle, $P(x, y, \theta; t)$, which contains full information on the diffusive properties of the system. When evaluated at the CoH, the translational and orientational distributions can be separated, and both have a Gaussian structure. The Gaussian PDF can then be transformed to another reference point. The 2D position PDFs, plotted in Fig. 12 for the reference point P chosen outside of the body for illustration, are obtained by integrating out the orientational degree of freedom. We clearly see that this specific choice of the reference point renders PDFs which significantly deviate from the Gaussian distribution. After evaluating the PDFs at P numerically, we provide an analytical expression for the case when the drag (or the diffusion tensor) is isotropic using the Jacobi-Anger expansion. Both these results replicate the experimental PDFs with no free parameters, with the diffusion coefficient being the only input. Our result emphasises that Gaussian statistics do not apply when tracking off the CoH and provide direct interpretation for the measurements. Furthermore, the procedure highlighted in the paper, and the results therein, are generally applicable to any particle undergoing two-dimensional Brownian motions.

3. Summary

In conclusion, the realization of the projects constituting the presented scientific Achievement has led to a number of interesting conclusions regarding the near-interface dynamics of colloidal particles, microscopic artificial swimmers, diffusion in the presence of boundaries, and the theoretical tools that are available to interpret the experimental data. The results are interesting from the fundamental point of view, since we have developed novel predictions for a number of systems that invite further studies. From an applied research perspective, our findings prove useful for the design of microfluidic systems, where interfacial flows are the dominant shaping mechanism, and in the design of bio-mimetic artificial microswimmers. The presented theoretical results explained, guided and inspired ongoing and upcoming experimental works. Our works contribute towards a better understanding of the fundamental flow mechanisms at the microscopic scale.

At present, my efforts are directed towards establishing a research group and developing novel theoretical predictions for elastic filaments in microscale flows. I continue the studies of low Reynolds number flows in order to develop practical modelling tools. I have established a number of novel experimental collaborations and joint projects which benefit from the theoretical input provided by my ongoing efforts in the field of microscale fluid dynamics.

5 PRESENTATION OF SIGNIFICANT SCIENTIFIC OR ARTISTIC ACTIVITY CARRIED OUT AT MORE THAN ONE UNIVERSITY, SCIENTIFIC OR CULTURAL INSTITUTION, ESPECIALLY AT FOREIGN INSTITUTIONS

My other research activities involve a number of research collaborations. I started my research work in 2011 by graduating with an M.Sc. diploma at the University of Warsaw, followed by enrollment into a Ph.D project at the University of Warsaw under the supervision of Prof. Bogdan Cichocki, in collaboration with an experimental group of Prof. Jan Dhont at Forschungszentrum Jülich in Germany. I graduated with a Ph.D (*summa cum laude*) in 2015, and took up a David Crighton Fellowship and later a postdoctoral Mobility Plus Fellowship at the University of Cambridge. A major part of my work started in 2015 during my postdoctoral stay as a Research Fellow in the Department of Applied Mathematics and Theoretical Physics at the University of Cambridge, working closely with Prof. Eric Lauga, while also pursuing other collaborations. In 2019, I was appointed an Asisstant Professor at the Faculty of Physics, University of Warsaw, where I am in the process of establishing a research group and a laboratory. I maintain a broad range of (mostly international) collaborations with a number of researchers working in the United Kingdom and USA, with a number of ongoing projects.

The resulting publications [B1-B13] are listed below, in addition to the papers [A1-A9] which constitute the scientific achievement.

Articles [B11-B13] describe the research undertaken within the Ph.D. research under the supervision of Prof. Bogdan Cichocki. The project concerned the development of a theoretical framework necessary to interpret the results of evanescent wave dynamic light scattering (EWDLS) experiments, performed in the group of Prof. Jan Dhont and Peter Lang. The aim was to relate the scattered light intensity time-correlation function with the diffusive properties of the system. In classical dynamic light scattering experiments (DLS) [321], the decay rate of the mentioned correlation function enables one to determine the diffusion coefficient. In a wall-bounded geometry, EWDLS experiments allow to determine the near-wall diffusion coefficients of sub-micrometer colloidal particles. After graduating with a Ph.D. degree, I have published a paper [B10] which continues the line of work started within the doctoral project by extending the theoretical findings from a dilute system (realised within the Ph.D. project) to systems with a non-zero concentration of colloids. The paper resulted from a collaboration involving experiments, extensive numerical simulation, and theoretical predictions. My role was to develop the theoretical model and work simulation data to directly compare the predictions to experimental results.

In the book chapter [B9], I worked with Gerhard Nägele to provide an overview of interfacial effects in colloidal systems. The chapter discusses hydrodynamic interactions in Stokes flow, introduces the notions of friction and mobility, and provides a description of many-body hydrodynamic interactions. In addition, we provide insights into the physics of active systems by discussing the problem of phoretic motion and microscale swimming.

In the article [B8], together with Eric Lauga and Sebastien Michelin, we discuss the problem of diffusiophoretic flow caused by the chemical activity of surfaces in a confined geometry. In this context, we propose a microscale pumping or stirring mechanism in a channel formed by two eccentric cylinders. The inner cylinder, being chemically active, releases or absorbs solute. The geometric asymmetry is sufficient to create a steady concentration gradient in the space between the cylinders, which drives a Stokes flow. We analyse the structure of this flow and describe the optimal geometric arrangement which maximises the flux of the circulating fluid.

In the article [B7], with A. Daddi-Moussa-Ider and Stephan Gekle, we derive the Green's function for a point force acting in a viscous fluid in the vicinity of a spherical capsule made of an elastic membrane for the case when the point force is non-radial. In this way, we extend the previous results obtained for a no-slip rigid spherical surface and quantify the velocity field depending on the geometry of the system and the temporal characteristics of motion. We derive analytical expressions for the leading-order hydrodynamic mobility of a small solid particle undergoing motion tangential to a nearby large spherical capsule whose membrane possesses resistance toward shearing and bending. We find a low-frequency peak in the particle

self-mobility resulting from the shearing resistance of the membrane. We also determine the in-plane mean-square displacement for a small particle diffusing nearby and find that the membrane induces a long-range subdiffusive regime of motion. We also consider the resulting motion of the capsule by finding a correction to the pair-mobility function. Our analytical calculations favourably compare with our fully resolved boundary integral simulations.

In the articles [B5] and [B6], with A. Daddi-Moussa-Ider and Stephan Gekle, we focus on the problem of motion of a small colloid inside an elastic tube. Elastic channels are an important part of numerous soft matter systems, in which hydrodynamic interactions with membranes determine the behavior of particles. In Ref. [B5], we derive analytical expressions for Green's functions associated with a point-force directed parallel or perpendicular to the axis of a cylindrical channel, the walls of which exhibit resistance against shearing and bending. We use it to determine the leading order self- and pair mobility functions of particles placed on the channel symmetry axis. We find that the mobilities are primarily determined by the membrane shearing, while bending plays an insignificant role. We also compute and quantify the membrane deformation. Our fully analytical calculations of the Green's functions inside an elastic cylinder can be used as a building block for future analysis of transport in channels. In Ref. [B6], we additionally present an analytical calculation of the rotational mobility of a collodial particle revolving on the centerline of an elastic tube. We find that the correction to the rotational mobility for rotation about the cylinder axis depends only on the membrane shearing properties, while both shearing and bending contribute to the rotational mobility about a radial axis, perpendicular to the cylinder axis. We further show a coupling between shearing and bending for the rotation along the cylinder radial axis. In both cases, the results are verified by an excellent agreement with boundary integral simulations.

In the article [B4], together with S.Y. Reigh and E. Lauga, we address the problem of motion of spherical particle with a chemically active surface. This is inspired by Janus particles with the ability to move phoretically in self-generated chemical concentration gradients, which are model systems for active matter. They typically move in straight lines, reorienting only by rotational diffusion. In our contribution, we show theoretically that by a pre-designed surface coverage of both activity and mobility, controlled translational and rotational motion can be induced. This results in helical trajectories of these autonomous swimmers, where the pitch and radius can be controlled. Building on the classical mathematical framework of diffusiophoretic motion under a fixed-flux chemical boundary condition, we calculate the most general three-dimensional motion for an arbitrary surface coverage of a spherical particle. After illustrating our results on surface distributions, we next introduce a simple intuitive patch model to serve as a guide for designing arbitrary phoretic spheres in experimental implementations.

In the article [B3], together with M. Velho-Rodrigues, R. Goldstein, and E. Lauga we present a theoretical approach to quantifying biological diversity by characterising the statistical distribution of specific properties of a taxonomic group or habitat. We focus on motile microorganisms living in fluid environments, which exploit propulsion resulting from a variety of shapes and swimming strategies. In a unifying approach, we explore the variability of swimming speed for unicellular eukaryotes based on published and available data. We see that the data naturally partition into two categories: that from flagellates (with a small number of flagella) and from ciliates (with a much larger number). Despite the morphological differences between these groups, each of the two probability distributions of swimming speed are accurately represented by log-normal distributions, which we explore in detail. Moreover, we find that scaling of the distributions by a characteristic speed for each data set leads to a collapse onto an apparently universal distribution. Our results might suggest a universal way for ecological niches to be populated by abundant microorganisms. This line of thought is now being continued in an ongoing collaboration.

In the article [B2], in collaboration with A. Daddi-Moussa-Ider, H. Löwen and A. Menzel, we propose a minimal model to explore the dynamics of a microswimmer rigidly attached to a large microplatelet, represented by a thin circular disk. This was inspired by one of the strategies being used to guide active microswimmers to predefined target location, thereby realizing microscale complex transport, which relied on attaching

a microswimmer to a passive component orientable by an external field. To analyse the model, we determine the flow field induced by a Stokeslet that is located above the center of a spatially fixed rigid disk of no-slip surface conditions. Then we determine and analyze possible trajectories of the overall composite. To explore the capability of external guidance, the platelet is additionally endowed with a permanent magnetic moment, which couples to a homogeneous external magnetic field. As previous experimental studies suggest, related setups may be helpful to guide sperm cells, or for targeted drug delivery.

The article [B1], in a large collaboration, offers a theoretical analysis of the motion of a self-propelled microswimmer moving inside a clean viscous drop or a drop covered with a homogeneously distributed surfactant. This is inspired by biological examples in which confinement strongly affects the stability and transport properties of active suspensions. Here, we describe the interfacial viscous stresses induced by the surfactant using the Boussinesq-Scriven constitutive rheological model. The active swimmer inside the droplet is represented by a force dipole and the resulting fluid-mediated hydrodynamic couplings between the swimmer and the confining drop are investigated. We find that the presence of the surfactant significantly influences the dynamics of the entrapped swimmer by enhancing its reorientation capability. We present exact solutions for the hydrodynamic image system for the Stokeslet and dipolar flow singularities inside the drop, both of which are represented by infinite series of harmonic components. Our results provide insights into guiding principles for the control of confined active matter systems.

List of publications not included as the Achievement in Sec. 4

[B1] A.R. Sprenger, V.A. Shaik, A.M. Ardekani, **M. Lisicki**, A.J.T.M. Mathijssen, F. Guzmán-Lastra, H. Löwen, A.M. Menzel, A. Daddi-Moussa-Ider,
Towards an analytical description of active microswimmers in clean and in surfactant-covered drops,
Eur. Phys. J. E **43**, 58 (2020).

[B2] A. Daddi-Moussa-Ider, **M. Lisicki**, H. Löwen, A.M. Menzel
Dynamics of a microswimmer-microplatelet composite,
Phys. Fluids **32**, 021902 (2020).

[B3] **M. Lisicki**, M.F. Velho Rodrigues, R.E. Goldstein, E. Lauga,
Swimming eukaryotic microorganisms exhibit a universal speed distribution
eLife **8**, e44907 (2019).

[B4] **M. Lisicki**, S.Y. Reigh, E. Lauga,
Autophoretic motion in three dimensions
Soft Matter **14**, 3304-3314 (2018).

[B5] A. Daddi-Moussa-Ider, **M. Lisicki**, S. Gekle,
Hydrodynamic mobility of a sphere moving on the centerline of an elastic tube,
Phys. Fluids **29**, 111901 (2017). Selected as *Editor's Pick 2017*

[B6] A. Daddi-Moussa-Ider, **M. Lisicki**, S. Gekle,
Slow rotation of a spherical particle inside an elastic tube
Acta Mech. **229**, 149-171 (2017).

[B7] A. Daddi-Moussa-Ider, **M. Lisicki**, S. Gekle,
Hydrodynamic mobility of a solid particle nearby a spherical elastic membrane. II. Asymmetric motion
Phys. Rev. E **95**, 053117 (2017).

[B8] **M. Lisicki**, S. Michelin, E. Lauga,
Phoretic flow induced by asymmetric confinement,
J. Fluid Mech. **799**, R5 (2016).

[B9] **M. Lisicki**, G. Nägele,
Colloidal hydrodynamics and interfacial effects,
in: Soft Matter at Aqueous Interfaces, P. R. Lang and Y. Liu (eds.), Lecture Notes in Physics, vol. **917**, 313-386, Springer (2016).

[B10] Y. Liu, J. Bławzdziewicz, B. Cichocki, J.K.G. Dhont, **M. Lisicki**, E. Wajnryb, Y.N. Young, P.R. Lang,
Near-Wall dynamics of concentrated hard-sphere suspensions: comparison of evanescent wave DLS experiments, virial approximation and simulations,
Soft Matter **11**, 7316 (2015).

[B11] **M. Lisicki**, B. Cichocki, S.A. Rogers, J.K.G. Dhont, P.R. Lang,
Translational and rotational near-wall diffusion of spherical colloids studied by evanescent wave scattering,
Soft Matter **10**, 4312 (2014).

[B12] S.A. Rogers, **M. Lisicki**, B. Cichocki, J.K.G. Dhont, P.R. Lang,
Rotational diffusion of spherical colloids close to a wall,
Phys. Rev. Lett. **109**, 098305 (2012).

[B13] **M. Lisicki**, B. Cichocki, J.K.G. Dhont, P.R. Lang,
One-particle correlation function in evanescent wave dynamic light scattering,
J. Chem. Phys. **136**, 204704 (2012).

6 PRESENTATION OF TEACHING AND ORGANIZATIONAL ACHIEVEMENTS AS WELL AS ACHIEVEMENTS IN POPULARIZATION OF SCIENCE OR ART

A. TEACHING EXPERIENCE

2019 – Lectures and examples classes at the University of Warsaw. Regular teaching duties of an Assistant Professor. Courses taught: Statistical Physics (4th year; lectures and classes), Physics of Biological Systems (monographic lecture), Hydrodynamics and Elasticity (4th year), Advanced Hydrodynamics (monographic lecture).

2016 – 2018 Supervisions (undergraduate tutorials) in Statistical Physics (3rd year), Differential Equations (1st year), Variational Principles (2nd year) , Methods (2nd year), and Fluid Dynamics (2nd year) at Department of Applied Mathematics and Theoretical Physics (DAMTP) and Trinity College, University of Cambridge; ca. 60 students in total.

2013 – 2014 Examples classes in undergraduate courses: Mechanics of Continuous Media (3rd year) and Calculus (2nd year), Faculty of Physics, University of Warsaw. Awarded the Dean's Prize for Teaching in the academic year 2013/2014.

B. ORGANIZATIONAL ACTIVITY

- President of Trinity College Post Doctoral Society (2017/2018), an organisation gathering over 100 postdocs in Trinity College at the University of Cambridge.
- Member of the networking group COST Action MP1305 Flowing Matter.
- Member of the Polish Physics Olympiad Main Committee, since September 2011. Responsible for selecting and discussing theoretical and experimental problems for the competition.

- Main organiser (together with E. Lauga) of Complex Motion in Fluids 2017 School in Girton College, University of Cambridge.
- Member of the Organising Committee of 6th Warsaw School of Statistical Physics (2016) and the forthcoming 7th Warsaw School of Statistical Physics (2022).

C. SCIENCE POPULARIZATION

Popular science talks and conferences:

- Speaker at TEDx Warsaw Women event in November 2020. Talk *Simplicity and complexity* is available on YouTube.
- Author of an educational video *Kitchen and bathroom fluid mechanics* (in Polish), within a University of Warsaw educational series for high school students.
- Selected speaker at Science: Polish Perspectives conference in Cambridge (2017). Awarded the Best Presentation Award.
- Poster presenter at Science: Polish Perspectives conference in Cambridge (2015).
- Popular science talks: Grammar School No. 5 in Legionowo (2016), Polish Science Cafe at University of Cambridge (2016), Science Festival (Warsaw, 2020).
- Participant in the New Scientist Live: a yearly popular science event in London, UK, 2017.
- Participant in the Polish Radio Science Fair: an open-air yearly event in Warsaw, Poland, 2011, 2013.
- Physics expert for radio and TV programmes (5 interviews for the Polish Radio, 2 for the Polish TV).

Popular science articles and other works:

[C1] M. Lisicki, *Cząstki Janusa, syntetyczne pływaki i materia aktywna w mikroskali*, Postępy Fizyki **3**, 2020/

[C2] M. Lisicki, *W lepkim mikroświecie: krótka lekcja pływania w miodzie*, Postępy Fizyki **1**, 2019.

[C3] M. Lisicki, *W pół drogi do nieskończoności [Halfway to infinity]*, Delta **7**, 2013.

[C4] M. Lisicki, *Dlaczego woda wylewa się z wiadra? [Why does water pour out from a bucket?]*, Delta **10**, 2010.

[C5] M. Lisicki, *O rysowaniu zderzeń [On drawing collisions]*, Delta **3**, 2010.

[C6] M. Lisicki, *Fatamorgana w miniaturze [Mirage in miniature]*, Delta **10**, 2008.

[C7] M. Lisicki, *Four approaches to hydrodynamic Green's functions - the Oseen tensors*, `https://arxiv.org/abs/1312.6231` (2013).

The paper **[C1]** received the 1st prize in the journal competition for the best popular science article organized by the Polish Physical Society.

7 OTHER PROFESSIONAL INFORMATION

- I am currently a co-advisor of a graduate student, Mr. Radost Waszkiewicz, since 09.2019. The PhD scholarship is funded from the NCN Sonata grant, *Dynamic deformation of elastic filaments in viscous fluids*, of which I am the Principal Investigator.
- Laureate of a START scholarship, awarded in 2017 by the Foundation for Polish Science (FNP) in recognition of scientific achievements.
- Laureate of the Polish Ministry of Science Award for Educational Excellence for the academic year 2010/2011, 2009/2010 and 2008/2009.

Maciej Lisicki

References

[1] M. Doi, *Soft Matter Physics* (Oxford Univ. Press, 2013).

[2] J. Mewis and N. J. Wagner, *Colloidal suspension rheology* (Cambridge University Press, 2012).

[3] P. M. Chaikin and T. C. Lubensky, *Principles of condensed matter physics*, Vol. 1 (2000).

[4] P. G. de Gennes, Soft Matter **1**, 16 (2005).

[5] J. K. G. Dhont, *An introduction to dynamics of colloids* (Elsevier, 1996).

[6] E. Guazzelli and J. F. Morris, *A Physical Introduction to Suspension Dynamics* (Cambridge Univ. Press, 2012).

[7] J. Happel and H. Brenner, *Low Reynolds number hydrodynamics: with special applications to particulate media*, Vol. 1 (Springer Science & Business Media, 2012).

[8] T. Squires and S. Quake, Rev. Mod. Phys. **77**, 977 (2005).

[9] P. Gravesen, J. Branebjerg, and O. S. Jensen, J. Micromech. Microeng. **3**, 168 (1993).

[10] J. Agudo-Canalejo and R. Lipowsky, Biophys. J. **110**, 189a (2016).

[11] N. G. Van Kampen, *Stochastic Processes in Physics and Chemistry*, 3rd ed. (Elsevier, 2001).

[12] S. Kim and S. J. Karrila, *Microhydrodynamics: Principles and Selected Applications* (Butterworth- Heinemann, Boston, 1991).

[13] M. L. Ekiel-Jeżewska and E. Wajnryb, in *Theoretical Methods for Micro Scale Viscous Flows*, edited by F. Feuillebois and A. Sellier (2009) pp. 127–172.

[14] M. Lisicki, arXiv:1312.6231 [physics.flu-dyn] (2013), arXiv:1312.6231 .

[15] J. Rotne and S. Prager, J. Chem. Phys. **50**, 4831 (1969).

[16] H. Yamakawa, J. Chem. Phys. **53**, 436 (1970).

[17] P. J. Zuk, E. Wajnryb, K. A. Mizerski, and P. Szymczak, J. Fluid Mech. **741**, R5 (2014).

[18] P. J. Zuk, B. Cichocki, and P. Szymczak, Biophys. J. **115**, 782 (2018).

[19] J. F. Brady and G. Bossis, Annu. Rev. Fluid Mech. **20**, 111 (1988).

[20] G. Perkins and R. B. Jones, Physica A **171**, 575 (1991).

[21] H. A. Lorentz, *Abhandlung über Theoretische Physik* (B. G. Teubner, Leipzig und Berlin, 1907).

[22] J. Blake, Proc. Camb. Phil. Soc. **70**, 303 (1971).

[23] B. Cichocki, R. B. Jones, R. Kutteh, and E. Wajnryb, J. Chem. Phys. **112**, 2548 (2000).

[24] D. Lopez and E. Lauga, Phys. Fluids **26**, 071902 (2014).

[25] J. R. Blake, Math. Proc. Camb. Phil. Soc. **70**, 303 (1971).

[26] G. Perkins and R. Jones, Physica A **171**, 575 (1991).

[27] B. U. Felderhof, J. Phys. Chem. B **109**, 21406 (2005).

[28] B. Felderhof, J. Chem. Phys. **123**, 184903 (2005).

[29] B. Cichocki and R. B. Jones, Physica A **258**, 273 (1998).

[30] J. W. Swan and J. F. Brady, Phys. Fluids **19**, 113306 (2007).

[31] J. W. Swan and J. F. Brady, Phys. Fluids **22**, 103301 (2010).

[32] T. Franosch and S. Jeney, Phys. Rev. E **79**, 031402 (2009).

[33] S. H. Lee, R. S. Chadwick, and L. G. Leal, J. Fluid Mech. **93**, 705 (1979).

[34] S. H. Lee and L. G. Leal, J. Fluid Mech. **98**, 193 (1980).

[35] C. Berdan II and L. G. Leal, J. Colloid Interface Sci. **87**, 62 (1982).

[36] J. Urzay, S. G. Llewellyn Smith, and B. J. Glover, Phys. Fluids **19**, 103106 (2007).

[37] E. Lauga and T. M. Squires, Physics of Fluids (1994-present) **17**, 103102 (2005).

[38] E. Lauga, M. Brenner, and H. Stone, in *Springer handbook of experimental fluid mechanics* (Springer, 2007) pp. 1219–1240.

[39] B. U. Felderhof, Phys. Rev. E **85**, 046303 (2012).

[40] B. Felderhof, J. Chem. Phys. **124**, 124705 (2006).

[41] A. J. T. M. Mathijssen, A. Doostmohammadi, J. M. Yeomans, and T. N. Shendruk, J. Fluid Mech. **806**, 35 (2016).

[42] R. A. Lambert, F. Picano, W.-P. Breugem, and L. Brandt, J. Fluid Mech. **733**, 528 (2013).

[43] A. Banerjee and K. Kihm, Phys. Rev. E **72**, 042101 (2005).

[44] K. D. Kihm, a. Banerjee, C. K. Choi, and T. Takagi, Exp. Fluids **37**, 811 (2004).

[45] D. C. Prieve, F. Lanni, and F. Luo, Faraday Discuss. Chem. Soc. **83**, 297 (1987).

[46] D. C. Prieve, Adv. Coll. Interf. Sci. **82**, 93 (1999).
[47] J. Y. Walz and L. Suresh, J. Chem. Phys. **103** (1995).
[48] B. Lin, J. Yu, and S. Rice, Phys. Rev. E **62**, 3909 (2000).
[49] K. H. Lan, N. Ostrowsky, and D. Sornette, Phys. Rev. Lett. **57**, 17 (1986).
[50] P. Holmqvist, J. K. G. Dhont, and P. R. Lang, Phys. Rev. E **74**, 021402 (2006).
[51] P. Holmqvist, J. K. G. Dhont, and P. R. Lang, J. Chem. Phys. **126**, 044707 (2007).
[52] M. Haghighi, M. N. Tahir, W. Tremel, H.-J. Butt, and W. Steffen, J. Chem. Phys. **139**, 064710 (2013).
[53] R. W. Verweij, S. Ketzetzi, J. de Graaf, and D. J. Kraft, Physical Review E **102** (2020), 10.1103/physreve.102.062608.
[54] W. Russel, E. Hinch, L. G. Leal, and G. Tieffenbruck, J. Fluid Mech **83**, 273 (1977).
[55] W. H. Mitchell and S. E. Spagnolie, J. Fluid. Mech. **772**, 600 (2015).
[56] D. Katz, J. Blake, and S. Paveri-Fontana, J. Fluid Mech , 529 (1975).
[57] S.-M. Yang and L. G. Leal, J. Fluid Mech. **136**, 393 (1983).
[58] N. J. De Mestre and W. B. Russel, J. Eng. Math. **9**, 81 (1975).
[59] R. Hsu and P. Ganatos, J. Fluid Mech. **207**, 29 (1989).
[60] M. De Corato, F. Greco, G. D'Avino, and P. L. Maffettone, J. Chem. Phys. **142**, 194901 (2015).
[61] J. T. Padding and W. J. Briels, J. Chem. Phys. **132**, 054511 (2010).
[62] J. García de la Torre and V. A. Bloomfield, Q. Rev. Biophys. **14**, 81 (1981).
[63] B. Cichocki, R. B. Jones, R. Kutteh, and E. Wajnryb, J. Chem. Phys. **112**, 2548 (2000).
[64] M. Wanunu, Physics of Life Reviews **9**, 125 (2012).
[65] D. Branton, D. W. Deamer, A. Marziali, H. Bayley, S. A. Benner, T. Butler, M. Di Ventra, S. Garaj, A. Hibbs, X. Huang, S. B. Jovanovich, P. S. Krstic, S. Lindsay, X. S. Ling, C. H. Mastrangelo, A. Meller, J. S. Oliver, Y. V. Pershin, J. M. Ramsey, R. Riehn, G. V. Soni, V. Tabard-Cossa, M. Wanunu, M. Wiggin, and J. A. Schloss, Nat Biotechnol **26**, 1146 (2008).
[66] S. E. Henrickson, M. Misakian, B. Robertson, and J. J. Kasianowicz, Phys. Rev. Lett. **85**, 3057 (2000).
[67] J. J. Kasianowicz, E. Brandin, D. Branton, and D. W. Deamer, Proc. Natl. Acad. Sci. USA **93**, 13770 (1996), https://www.pnas.org/content/93/24/13770.full.pdf .
[68] P. Waduge, R. Hu, P. Bandarkar, H. Yamazaki, B. Cressiot, Q. Zhao, P. C. Whitford, and M. Wanunu, *ACS Nano*, ACS Nano **11**, 5706 (2017).
[69] A. Meller, L. Nivon, and D. Branton, Phys. Rev. Lett. **86**, 3435 (2001).
[70] C. Forrey and M. Muthukumar, J. Chem. Phys. **127**, 015102 (2007), https://doi.org/10.1063/1.2746246 .
[71] Y. Ai and S. Qian, Phys. Chem. Chem. Phys. **13**, 4060 (2011).
[72] M. Muthukumar, J. Chem. Phys. **132**, 195101 (2010), https://doi.org/10.1063/1.3429882 .
[73] M. M. Hatlo, D. Panja, and R. van Roij, Phys. Rev. Lett. **107**, 068101 (2011).
[74] B.-J. Jeon and M. Muthukumar, J. Chem. Phys. **140**, 015101 (2014), https://doi.org/10.1063/1.4855075 .
[75] P. Szymczak, The European Physical Journal Special Topics **223**, 1805 (2014).
[76] A. Y. Grosberg and Y. Rabin, J. Chem. Phys. **133**, 165102 (2010), https://doi.org/10.1063/1.3495481 .
[77] L. Qiao, M. Ignacio, and G. W. Slater, J. Chem. Phys. **151**, 244902 (2019), https://doi.org/10.1063/1.5134076 .
[78] L. Qiao and G. W. Slater, J. Chem. Phys. **152**, 144902 (2020).
[79] J. Happel and H. Brenner, *Low Reynolds Numbers Hydrodynamics* (Kluwer, Dordrecht, 1991).
[80] Z. Dogic and S. Fraden, Phil. Trans. Roy. Soc. London. Ser. A **359**, 997 (2001), https://royalsocietypublishing.org/doi/pdf/10.1098/rsta.2000.0814 .
[81] A. McMullen, H. W. de Haan, J. X. Tang, and D. Stein, Nature Communications **5**, 4171 (2014).
[82] H. W. de Haan and G. W. Slater, Phys. Rev. Lett. **110**, 048101 (2013).
[83] R. Kumar Sharma, I. Agrawal, L. Dai, P. S. Doyle, and S. Garaj, Nature Communications **10**, 4473 (2019).
[84] S. Naahidi, M. Jafari, F. Edalat, K. Raymond, A. Khademhosseini, and P. Chen, Journal of controlled release **166**, 182 (2013).
[85] H. Al-Obaidi and A. T. Florence, Journal of Drug Delivery Science and Technology **30**, 266 (2015).
[86] J. Liu, T. Wei, J. Zhao, Y. Huang, H. Deng, A. Kumar, C. Wang, Z. Liang, X. Ma, and X.-J. Liang, Biomaterials **91**, 44 (2016).
[87] G. J. Doherty and H. T. McMahon, Annu. Rev. Biochem. **78**, 857 (2009).

[88] A. Meinel, B. Tränkle, W. Römer, and A. Rohrbach, Soft matter **10**, 3667 (2014).
[89] J. Agudo-Canalejo and R. Lipowsky, ACS Nano **9**, 3704 (2015).
[90] H. A. Lorentz, Abh. Theor. Phys. **1**, 23 (1907).
[91] T. Bickel, Eur. Phys. J. E **20**, 379 (2006).
[92] T. Bickel, Phys. Rev. E **75**, 041403 (2007).
[93] G. M. Wang, R. Prabhakar, and E. M. Sevick, Phys. Rev. Lett. **103**, 248303 (2009).
[94] J. Bławzdziewicz, M. Ekiel-Jeżewska, and E. Wajnryb, J. Chem. Phys. **133**, 114703 (2010).
[95] J. Bławzdziewicz, M. L. Ekiel-Jeżewska, and E. Wajnryb, J. Chem. Phys. **133** (2010).
[96] T. Bickel, EPL (Europhys. Lett.) **106**, 16004 (2014).
[97] B. U. Felderhof, J. Chem. Phys. **125**, 144718 (2006).
[98] B. U. Felderhof, J. Chem. Phys. **125**, 124904 (2006).
[99] T. Salez and L. Mahadevan, J. Fluid Mech. **779**, 181 (2015).
[100] R. Shlomovitz, A. Evans, T. Boatwright, M. Dennin, and A. Levine, Phys. Rev. Lett. **110**, 137802 (2013).
[101] R. Shlomovitz, A. A. Evans, T. Boatwright, M. Dennin, and A. J. Levine, Phys. Fluids **26** (2014).
[102] A. Daddi-Moussa-Ider, A. Guckenberger, and S. Gekle, Phys. Rev. E **93**, 012612 (2016).
[103] A. Daddi-Moussa-Ider, A. Guckenberger, and S. Gekle, Phys. Fluids **28**, 071903 (2016).
[104] A. Daddi-Moussa-Ider and S. Gekle, J. Chem. Phys. **145**, 014905 (2016).
[105] B. Saintyves, T. Jules, T. Salez, and L. Mahadevan, Proc. Nat. Acad. Sci. **113**, 5847 (2016).
[106] L. P. Faucheux and A. J. Libchaber, Phys. Rev. E **49**, 5158 (1994).
[107] B. Lin, J. Yu, and S. A. Rice, Phys. Rev. E **62**, 3909 (2000).
[108] E. R. Dufresne, D. Altman, and D. G. Grier, EPL (Europhys. Lett.) **53**, 264 (2001).
[109] E. Schäffer, S. F. Nørrelykke, and J. Howard, Langmuir **23**, 3654 (2007).
[110] H. B. Eral, J. M. Oh, D. van den Ende, F. Mugele, and M. H. G. Duits, Langmuir **26**, 16722 (2010).
[111] A. E. Cervantes-Martínez, A. Ramírez-Saito, R. Armenta-Calderón, M. A. Ojeda-López, and J. L. Arauz-Lara, Phys. Rev. E **83**, 030402 (2011).
[112] S. L. Dettmer, S. Pagliara, K. Misiunas, and U. F. Keyser, Phys. Rev. E **89**, 062305 (2014).
[113] T. Boatwright, M. Dennin, R. Shlomovitz, A. A. Evans, and A. J. Levine, Phys. Fluids **26**, 071904 (2014).
[114] F. Jünger, F. Kohler, A. Meinel, T. Meyer, R. Nitschke, B. Erhard, and A. Rohrbach, Biophys. J. **109**, 869 (2015).
[115] B. Tränkle, D. Ruh, and A. Rohrbach, Soft matter **12**, 2729 (2016).
[116] M. Irmscher, A. M. de Jong, H. Kress, and M. W. J. Prins, Biophysical journal **102**, 698 (2012).
[117] F. Perrin, J. Phys. Radium **5**, 497 (1934).
[118] F. Perrin, J. Phys. Radium **7**, 1 (1936).
[119] G. K. Batchelor, J. Fluid Mech. **44**, 419 (1970).
[120] R. Cox, J. Fluid Mech. **44**, 791 (1970).
[121] J. B. Keller and S. I. Rubinow, J. Fluid Mech. **75**, 705 (1976).
[122] A. T. Chwang and T. Y.-T. Wu, J. Fluid Mech. **67**, 787 (1975).
[123] N. J. De Mestre and W. B. Russel, J. Eng. Math. **9**, 81 (1975).
[124] D. Schiby and I. Gallily, J. Colloid Interface Sci. **77**, 328 (1980).
[125] W. H. Mitchell and S. E. Spagnolie, J. Fluid Mech. **772**, 600 (2015).
[126] J. R. Blake and G. R. Fulford, Bull. Aust. Math. Soc. **24**, 27 (1981).
[127] Y. Han, A. M. Alsayed, M. Nobili, J. Zhang, T. C. Lubensky, and A. G. Yodh, Science **314**, 626 (2006).
[128] Y. Han, A. Alsayed, M. Nobili, and A. G. Yodh, Phys. Rev. E **80**, 011403 (2009).
[129] Z. Zheng and Y. Han, J. Chem. Phys. **133**, 124509 (2010).
[130] G. Li and J. X. Tang, Phys. Rev. E **69**, 061921 (2004).
[131] R. Duggal and M. Pasquali, Phys. Rev. Lett. **96**, 246104 (2006).
[132] B. Bhaduri, A. Neild, and T. W. Ng, Applied Physics Letters **92**, 084105 (2008).
[133] F. C. Cheong and D. G. Grier, Optics express **18**, 6555 (2010).
[134] R. Colin, M. Yan, L. Chevry, J.-F. Berret, and B. Abou, EPL (Europhys. Lett.) **97**, 30008 (2012).
[135] D. Mukhija and M. J. Solomon, J. Colloid Interface Sci. **314**, 98 (2007).
[136] R. Skalak, A. Tozeren, R. P. Zarda, and S. Chien, Biophys. J. **13(3)**, 245 (1973).

[137] T. Krüger, F. Varnik, and D. Raabe, Computers and Mathematics with Applications **61**, 3485 (2011).
[138] T. Krüger, *Computer simulation study of collective phenomena in dense suspensions of red blood cells under shear* (Springer Science & Business Media, 2012).
[139] T. Krüger, D. Holmes, and P. V. Coveney, Biomicrofluidics **8**, 054114 (2014).
[140] S. Gekle, Biophys. J. **110**, 514 (2016).
[141] W. Helfrich, Z. Naturf. C. **28:693** (1973).
[142] D. Abreu, M. Levant, V. Steinberg, and U. Seifert, Adv. Colloid Interface Sci. **208**, 129 (2014).
[143] E. Lauga, W. R. DiLuzio, G. M. Whitesides, and H. A. Stone, Biophys. J. **90**, 400 (2006).
[144] D. Lopez and E. Lauga, Phys. Fluids **26**, 400 (2014).
[145] C. Bechinger, R. Di Leonardo, H. Löwen, C. Reichhardt, G. Volpe, and G. Volpe, Rev. Mod. Phys. **88**, 045006 (2016).
[146] J. Zhang, E. Luijten, B. A. Grzybowski, and S. Granick, Chemical Society Reviews **46**, 5551 (2017).
[147] A. Zöttl and H. Stark, Journal of Physics: Condensed Matter **28**, 253001 (2016).
[148] C. Chen, F. Soto, E. Karshalev, J. Li, and J. Wang, Adv. Funct. Mater. **29**, 1806290 (2019).
[149] D. A. Wilson, R. J. Nolte, and J. C. Van Hest, Nature Chemistry **4**, 268 (2012).
[150] J. García-Torres, C. Calero, F. Sagués, I. Pagonabarraga, and P. Tierno, Nature Communications **9**, 1663 (2018).
[151] L. Zhang, J. J. Abbott, L. Dong, B. E. Kratochvil, D. Bell, and B. J. Nelson, Applied Physics Letters **94**, 064107 (2009).
[152] J. R. Gomez-Solano, S. Samin, C. Lozano, P. Ruedas-Batuecas, R. van Roij, and C. Bechinger, Sci. Rep. **7**, 14891 (2017).
[153] A. F. Demirörs, F. Eichenseher, M. J. Loessner, and A. R. Studart, Nature Communications **8**, 1872 (2017).
[154] H. R. Vutukuri, B. Bet, R. Van Roij, M. Dijkstra, and W. T. Huck, Sci. Rep. **7**, 16758 (2017).
[155] R. Golestanian, T. B. Liverpool, and A. Ajdari, New J. Phys. **9**, 126 (2007).
[156] P. Mandal, G. Patil, H. Kakoty, and A. Ghosh, Accounts of Chemical Research **51**, 2689 (2018), https://doi.org/10.1021/acs.accounts.8b00315 .
[157] A. Yethiraj and A. van Blaaderen, Nature **421**, 513 (2003).
[158] O. D. Velev and K. H. Bhatt, Soft Matter **2**, 738 (2006).
[159] H. R. Vutukuri, Z. Preisler, T. H. Besseling, A. van Blaaderen, M. Dijkstra, and W. T. S. Huck, Soft Matter **12**, 9657 (2016).
[160] Y. Ji, X. Lin, H. Zhang, Y. Wu, J. Li, and Q. He, Angewandte Chemie International Edition **58**, 4184 (2019).
[161] Y. Wu, A. D. Kaiser, Y. Jiang, and M. S. Alber, Proceedings of the National Academy of Sciences **106**, 1222 (2009), https://www.pnas.org/content/106/4/1222.full.pdf .
[162] K. Son, J. S. Guasto, and R. Stocker, Nature physics **9**, 494 (2013).
[163] Y. Magariyama, S.-y. Masuda, Y. Takano, T. Ohtani, and S. Kudo, FEMS Microbiology Letters **205**, 343 (2001).
[164] O. Sliusarenko, J. Neu, D. R. Zusman, and G. Oster, Proceedings of the National Academy of Sciences **103**, 1534 (2006), https://www.pnas.org/content/103/5/1534.full.pdf .
[165] L. Xie, T. Altindal, S. Chattopadhyay, and X.-L. Wu, Proceedings of the National Academy of Sciences **108**, 2246 (2011).
[166] Y. Yuan, Q. Liu, B. Senyuk, and I. I. Smalyukh, Nature **570**, 214 (2019).
[167] A. Varma, T. D. Montenegro-Johnson, and S. Michelin, Soft matter **14**, 7155 (2018).
[168] J. Anderson, Annu. Rev. Fluid Mech. **21**, 61–99 (1989).
[169] S. E. Spagnolie and E. Lauga, J. Fluid Mech. **700**, 105 (2012).
[170] J. Palacci, S. Sacanna, A. P. Steinberg, D. J. Pine, and P. M. Chaikin, Science **339**, 936 (2013), https://science.sciencemag.org/content/339/6122/936.full.pdf .
[171] K. Drescher, K. C. Leptos, I. Tuval, T. Ishikawa, T. J. Pedley, and R. E. Goldstein, Phys. Rev. Lett. **102**, 168101 (2009).
[172] A. Domínguez, P. Malgaretti, M. N. Popescu, and S. Dietrich, Phys. Rev. Lett. **116**, 078301 (2016).
[173] C. Brennen and H. Winet, Ann. Rev. Fluid Mech. **9**, 339 (1977).
[174] E. Lauga, Ann. Rev. Fluid Mech. **48**, 105 (2016).
[175] E. Lauga and T. R. Powers, Rep. Prog. Phys. **72**, 096601 (2009).
[176] E. M. Purcell, Am. J. Phys. **45**, 3 (1977).

[177] J. D. Wheeler, E. Secchi, R. Rusconi, and R. Stocker, Ann. Rev. Cell. Develop. Biol. **35**, 213 (2019).
[178] R. Rusconi and R. Stocker, Curr. Opin. Microbiol. **25**, 1 (2015).
[179] A. P. Berke, L. Turner, H. C. Berg, and E. Lauga, Phys. Rev. Lett. **101**, 038102 (2008).
[180] E. Lauga, W. R. DiLuzio, G. M. Whitesides, and H. A. Stone, Biophys. J. **90**, 400 (2006).
[181] G. Miño, M. Baabour, R. Chertcoff, G. Gutkind, E. Clément, H. Auradou, and I. Ippolito, Adv. Microbiol. **8**, 451 (2018).
[182] J. O. Kessler, Nature **313**, 218 (1985).
[183] R. Rusconi, J. Guasto, and R. Stocker, Nat. Phys. **10**, 212 (2014).
[184] M. T. Barry, R. Rusconi, J. S. Guasto, and R. Stocker, J. R. Soc. Interface **12**, 20150791 (2015).
[185] W. R. DiLuzio, L. Turner, M. Mayer, P. Garstecki, D. B. Weibel, H. C. Berg, and G. M. Whitesides, Nature **435**, 1271 (2005).
[186] G. Grégoire and H. Chaté, Phys. Rev. Lett. **92**, 025702 (2004).
[187] S. Mishra, A. Baskaran, and M. C. Marchetti, Phys. Rev. E **81**, 061916 (2010).
[188] S. Heidenreich, S. Hess, and S. H. L. Klapp, Phys. Rev. E **83**, 011907 (2011).
[189] A. M. Menzel, Phys. Rev. E **85**, 021912 (2012).
[190] B. Liebchen, M. E. Cates, and D. Marenduzzo, Soft Matter **12**, 7259 (2016).
[191] T. Le Goff, B. Liebchen, and D. Marenduzzo, Phys. Rev. Lett. **117**, 238002 (2016).
[192] B. Liebchen and D. Levis, Phys. Rev. Lett. **119**, 058002 (2017).
[193] B. Liebchen, D. Marenduzzo, and M. E. Cates, Phys. Rev. Lett. **118**, 268001 (2017).
[194] A. M. Menzel, J. Physics: Condens. Matter **25**, 505103 (2013).
[195] F. Kogler and S. H. L. Klapp, Europhys. Lett. **110**, 10004 (2015).
[196] P. Romanczuk, H. Chaté, L. Chen, S. Ngo, and J. Toner, New J. Phys. **18**, 063015 (2016).
[197] A. M. Menzel, A. Saha, C. Hoell, and H. Löwen, J. Chem. Phys. **144**, 024115 (2016).
[198] J. Tailleur and M. E. Cates, Phys. Rev. Lett. **100**, 218103 (2008).
[199] J. Palacci, S. Sacanna, A. P. Steinberg, D. J. Pine, and P. M. Chaikin, Science **339**, 936 (2013).
[200] I. Buttinoni, J. Bialké, F. Kümmel, H. Löwen, C. Bechinger, and T. Speck, Phys. Rev. Lett. **110**, 238301 (2013).
[201] T. Speck, J. Bialké, A. M. Menzel, and H. Löwen, Phys. Rev. Lett. **112**, 218304 (2014).
[202] T. Speck, A. M. Menzel, J. Bialké, and H. Löwen, J. Chem. Phys. **142**, 224109 (2015).
[203] H. H. Wensink, J. Dunkel, S. Heidenreich, K. Drescher, R. E. Goldstein, H. Löwen, and J. M. Yeomans, Proc. Natl. Acad. Sci. **109**, 14308 (2012).
[204] H. H. Wensink and H. Löwen, J. Phys. Condens. Mat. **24**, 464130 (2012).
[205] J. Dunkel, S. Heidenreich, K. Drescher, H. H. Wensink, M. Bär, and R. E. Goldstein, Phys. Rev. Lett. **110**, 228102 (2013).
[206] S. Heidenreich, S. H. L. Klapp, and M. Bär, J. Phys. Conf. Ser. **490**, 012126 (2014).
[207] A. Kaiser, A. Peshkov, A. Sokolov, B. ten Hagen, H. Löwen, and I. S. Aranson, Phys. Rev. Lett. **112**, 158101 (2014).
[208] S. Heidenreich, J. Dunkel, S. H. L. Klapp, and M. Bär, Phys. Rev. E **94**, 020601 (2016).
[209] H. Löwen, Eur. Phys. J. Special Topics **225**, 2319 (2016).
[210] E. M. Maldonado and M. I. Latz, Biol. Bull. **212**, 242 (2007), pMID: 17565113.
[211] A. J. T. M. Mathijssen, J. Culver, M. S. Bhamla, and M. Prakash, Nature **571**, 560 (2019).
[212] J. Happel and B. J. Bryne, Industrial & Engineering Chemistry **46**, 1181 (1954).
[213] H. A. Stone, A. D. Stroock, and A. Ajdari, Annu. Rev. Fluid Mech. **36**, 381 (2004).
[214] B. Rallabandi, B. Saintyves, T. Jules, T. Salez, C. Schönecker, L. Mahadevan, and H. A. Stone, Phys. Rev. Fluids **2**, 074102 (2017).
[215] B. Rallabandi, S. Hilgenfeldt, and H. A. Stone, J. Fluid Mech. **818**, 407 (2017).
[216] A. Daddi-Moussa-Ider and S. Gekle, Phys. Rev. E **95**, 013108 (2017).
[217] P. D. Frymier, R. M. Ford, H. C. Berg, and P. T. Cummings, Proc. Natl. Acad. Sci. **92**, 6195 (1995).
[218] W. R. DiLuzio, L. Turner, M. Mayer, P. Garstecki, D. B. Weibel, H. C. Berg, and G. M. Whitesides, Nature **435**, 1271 (2005).
[219] K. Drescher, J. Dunkel, L. H. Cisneros, S. Ganguly, and R. E. Goldstein, Proc. Natl. Acad. Sci. **108**, 10940 (2011).

[220] G. Miño, T. E. Mallouk, T. Darnige, M. Hoyos, J. Dauchet, J. Dunstan, R. Soto, Y. Wang, A. Rousselet, and E. Clement, Phys. Rev. Lett. **106**, 048102 (2011).
[221] E. Lushi, V. Kantsler, and R. E. Goldstein, Phys. Rev. E **96**, 023102 (2017).
[222] K. Ishimoto and E. A. Gaffney, Phys. Rev. E **88**, 062702 (2013).
[223] M. Contino, E. Lushi, I. Tuval, V. Kantsler, and M. Polin, Phys. Rev. Lett. **115**, 258102 (2015).
[224] J. Dunstan, G. Miño, E. Clement, and S. Soto, Phys. Fluids **24**, 011901 (2012).
[225] S. Das, A. Garg, A. I. Campbell, J. Howse, A. Sen, D. Velegol, R. Golestanian, and S. J. Ebbens, Nat. Commun. **6** (2015).
[226] K. Schaar, A. Zöttl, and H. Stark, Phys. Rev. Lett. **115**, 038101 (2015).
[227] S. E. Spagnolie, G. R. Moreno-Flores, D. Bartolo, and E. Lauga, Soft Matter **11**, 3396 (2015).
[228] N. Desai, V. A. Shaik, and A. M. Ardekani, Soft matter (2018).
[229] H. Shum and J. M. Yeomans, Phys. Rev. Fluids **2**, 113101 (2017).
[230] M. C. van Loosdrecht, J. Lyklema, W. Norde, and A. J. Zehnder, Microbiol. Rev. , 75.
[231] K. Drescher, Y. Shen, B. L. Bassler, and H. A. Stone, Proc. Natl. Acad. Sci. **110**, 4345 (2013).
[232] W. E. Uspal, M. N. Popescu, S. Dietrich, and M. Tasinkevych, Soft Matter **11**, 6613 (2015).
[233] W. E. Uspal, M. N. Popescu, S. Dietrich, and M. Tasinkevych, Soft Matter **11**, 434 (2015).
[234] J. Simmchen, J. Katuri, W. E. Uspal, M. N. Popescu, M. Tasinkevych, and S. Sánchez, Nat. Commun. **7**, 10598 (2016).
[235] Y. Ibrahim and T. B. Liverpool, Europhys. Lett. **111**, 48008 (2015).
[236] A. Mozaffari, N. Sharifi-Mood, J. Koplik, and C. Maldarelli, Phys. Fluids **28**, 053107 (2016).
[237] M. N. Popescu, W. E. Uspal, and S. Dietrich, Eur. Phys. J. Special Topics **225**, 2189 (2016).
[238] F. Rühle, J. Blaschke, J.-T. Kuhr, and H. Stark, New J. Phys. (2017).
[239] A. Mozaffari, N. Sharifi-Mood, J. Koplik, and C. Maldarelli, Phys. Rev. Fluids **3**, 014104 (2018).
[240] D. Crowdy, S. Lee, O. Samson, E. Lauga, and A. E. Hosoi, J. Fluid Mech. **681**, 24 (2011).
[241] R. Di Leonardo, D. Dell'Arciprete, L. Angelani, and V. Iebba, Phys. Rev. Lett. **106**, 038101 (2011).
[242] M. C. Marchetti, J. F. Joanny, S. Ramaswamy, T. B. Liverpool, J. Prost, M. Rao, and R. A. Simha, Rev. Mod. Phys. **85**, 1143 (2013).
[243] J. Elgeti, R. G. Winkler, and G. Gompper, Reports Prog. Phys. **78** (2015).
[244] C. Bechinger, R. Di Leonardo, H. Löwen, C. Reichhardt, G. Volpe, and G. Volpe, Rev. Mod. Phys. **88**, 045006 (2016).
[245] A. Zöttl and H. Stark, J. Phys. Condens. Mat. **28**, 253001 (2016).
[246] A. Najafi and R. Golestanian, Phys. Rev. E **69**, 062901 (2004).
[247] A. Najafi and R. Golestanian, J. Phys. Condens. Mat. **17**, S1203 (2005).
[248] R. Golestanian and A. Ajdari, Phys. Rev. E **77**, 036308 (2008).
[249] R. Golestanian and A. Ajdari, Phys. Rev. Lett. **100**, 038101 (2008).
[250] G. P. Alexander, C. M. Pooley, and J. M. Yeomans, J. Phys. Condens. Matt. **21**, 204108 (2009).
[251] M. Leoni, J. Kotar, B. Bassetti, P. Cicuta, and M. C. Lagomarsino, Soft Matter **5**, 472 (2009).
[252] G. Grosjean, M. Hubert, G. Lagubeau, and N. Vandewalle, Phys. Rev. E **94**, 021101 (2016).
[253] A. Montino and A. DeSimone, Eur. Phys. J. E **38**, 42 (2015).
[254] E. Lauga, Soft Matter **7**, 3060 (2011).
[255] A. Montino and A. DeSimone, Acta Appl. Math. **149**, 53 (2017).
[256] J. Pande and A.-S. Smith, Soft Matter **11**, 2364 (2015).
[257] J. Pande, L. Merchant, T. Krüger, J. Harting, and A.-S. Smith, Soft Matter **13**, 3984 (2017).
[258] S. Babel, H. Löwen, and A. M. Menzel, Europhys. Lett. **113**, 58003 (2016).
[259] R. Ledesma-Aguilar, H. Löwen, and J. M. Yeomans, Eur. Phys. J. E **35**, 70 (2012).
[260] Dreyfus, R., Baudry, J., and Stone, H. A., Eur. Phys. J. B **47**, 161 (2005).
[261] M. S. Rizvi, A. Farutin, and C. Misbah, Phys. Rev. E **97**, 023102 (2018).
[262] B. U. Felderhof, Phys. Fluids **18**, 063101 (2006).
[263] O. S. Pak, L. Zhu, L. Brandt, and E. Lauga, Phys. Fluids **24**, 103102 (2012).
[264] L. Zhu, *Numerical investigation of swimming micro-organisms in complex environments* (KTH Royal Institute of Technology, 2012).

[265] M. P. Curtis and E. A. Gaffney, Phys. Rev. E **87**, 043006 (2013).
[266] S. Yazdi, A. M. Ardekani, and A. Borhan, Phys. Rev. E **90**, 043002 (2014).
[267] S. Yazdi, A. M. Ardekani, and A. Borhan, J. Nonlinear Sci. **25**, 1153 (2015).
[268] C. Datt, L. Zhu, G. J. Elfring, and O. S. Pak, J. Fluid Mech. **784** (2015).
[269] S. Yazdi and A. Borhan, Phys. Fluids **29**, 093104 (2017).
[270] D. Pimponi, M. Chinappi, P. Gualtieri, and C. M. Casciola, J. Fluid Mech. **789**, 514 (2016).
[271] A. Domínguez, P. Malgaretti, M. N. Popescu, and S. Dietrich, Phys. Rev. Lett. **116**, 078301 (2016).
[272] K. Dietrich, D. Renggli, M. Zanini, G. Volpe, I. Buttinoni, and L. Isa, New J. Phys. **19**, 065008 (2017).
[273] J. Elgeti and G. Gompper, Europhys. Lett. **85**, 38002 (2009).
[274] L. Zhu, E. Lauga, and L. Brandt, J. Fluid Mech. **726**, 285 (2013).
[275] F. Yang, S. Qian, Y. Zhao, and R. Qiao, Langmuir **32**, 5580 (2016).
[276] J. Elgeti and G. Gompper, Eur. Phys. J. Special Topics **225**, 2333 (2016).
[277] C. Liu, C. Zhou, W. Wang, and H. P. Zhang, Phys. Rev. Lett. **117**, 198001 (2016).
[278] G.-J. Li and A. M. Ardekani, Phys. Rev. E **90**, 013010 (2014).
[279] F. G. Woodhouse and R. E. Goldstein, Phys. Rev. Lett. **109**, 168105 (2012).
[280] H. Wioland, F. G. Woodhouse, J. Dunkel, J. O. Kessler, and R. E. Goldstein, Phys. Rev. Lett. **110**, 268102 (2013).
[281] H. Wioland, F. G. Woodhouse, J. Dunkel, and R. E. Goldstein, Nat. Phys. **12**, 341 (2016).
[282] F. G. Woodhouse and J. Dunkel, Nat. Commun. **8** (2017).
[283] A. J. T. M. Mathijssen, T. N. Shendruk, J. M. Yeomans, and A. Doostmohammadi, Phys. Rev. Lett. **116**, 028104 (2016).
[284] B. Cichocki and R. B. Jones, Physica A **258**, 273 (1998).
[285] N. Liron and S. Mochon, J. Eng. Math. **10**, 287 (1976).
[286] S. Bhattacharya and J. Bławzdziewicz, J. Math. Phys. **43**, 5720 (2002).
[287] S. Bhattacharya, J. Bławzdziewicz, and E. Wajnryb, J. Fluid Mech. **541**, 263 (2005).
[288] S. Bhattacharya, J. Bławzdziewicz, and E. Wajnryb, Physica A **356**, 294 (2005).
[289] J. de Graaf, A. J. T. M. Mathijssen, M. Fabritius, H. Menke, C. Holm, and T. N. Shendruk, Soft Matter **12**, 4704 (2016).
[290] R. Golestanian and A. Ajdari, Phys. Rev. E **77**, 036308 (2008).
[291] J. Dunkel, V. B. Putz, I. M. Zaid, and J. M. Yeomans, Soft Matter **6**, 4268 (2010).
[292] B. Nasouri, A. Vilfan, and R. Golestanian, Phys. Rev. Fluids **4**, 073101 (2019).
[293] J. Hill, O. Kalkanci, J. McMurry, and H. Koser, Phys. Rev. Lett. **98**, 068101 (2007).
[294] A. J. T. M. Mathijssen, N. Figueroa-Morales, G. Junot, É. Clément, A. Lindner, and A. Zöttl, Nat. Commun. **10**, 3434 (2019).
[295] R. Golestanian, Eur. Phys. J. E **25**, 1 (2008).
[296] Q. Brosseau, F. B. Usabiaga, E. Lushi, Y. Wu, L. Ristroph, J. Zhang, M. Ward, and M. J. Shelley, Phys. Rev. Lett. **123**, 178004 (2019).
[297] J. Palacci, S. Sacanna, A. Abramian, J. Barral, K. Hanson, A. Y. Grosberg, D. J. Pine, and P. M. Chaikin, Sci. Adv. **1**, e1400214 (2015).
[298] K. Miki and D. E. Clapham, Curr. Biol. **23**, 443 (2013).
[299] V. Kantsler, J. Dunkel, M. Blayney, and R. E. Goldstein, eLife , 02403 (2014).
[300] A. Chakrabarty, F. Wang, K. Sun, and Q.-H. Wei, Soft Matter **12**, 4318 (2016).
[301] A. Einstein, Ann. Phys. **322**, 549 (1905).
[302] M. Smoluchowski, Ann. Phys. **21**, 755 (1906).
[303] P. Langevin, C. R. Acad. Sci. **146**, 530 (1908).
[304] J. Perrin, Ann. Chim. Phys. **18**, 1 (1909).
[305] F. Perrin, J. Phys. le Radium **5**, 497 (1934).
[306] A. J. Goldman, R. G. Cox, and H. Brenner, Chem. Eng. Sci. **22**, 637 (1967).
[307] E. J. Hinch, J. Fluid Mech. **72**, 499 (1975).
[308] Y. Han, A. M. Alsayed, M. Nobili, J. Zhang, T. C. Lubensky, and A. G. Yodh, Science **314**, 626 (2006).
[309] A. V. Butenko, E. Mogilko, L. Amitai, B. Pokroy, and E. Sloutskin, Langmuir **28**, 12941 (2012).

[310] D. J. Kraft, R. Wittkowski, B. ten Hagen, K. V. Edmond, D. J. Pine, and H. Löwen, Phys. Rev. E **88**, 050301 (2013), 1305.1253 .

[311] A. Chakrabarty, A. Konya, F. Wang, J. V. Selinger, K. Sun, and Q.-H. Wei, Langmuir **30**, 13844 (2014).

[312] R. Huang, I. Chavez, K. M. Taute, B. Lukić, S. Jeney, M. G. Raizen, and E.-L. Florin, Nat. Phys. **7**, 576 (2011).

[313] A. Chakrabarty, F. Wang, C.-Z. Fan, K. Sun, and Q.-H. Wei, Langmuir **29**, 14396 (2013), pMID: 24171648, http://dx.doi.org/10.1021/la403427y .

[314] L. Koens and E. Lauga, Phys. Biol. **11**, 1 (2014).

[315] B. Cichocki, M. L. Ekiel-Jeżewska, and E. Wajnryb, J. Chem. Phys. **142**, 214902 (2015).

[316] B. Cichocki, M. L. Ekiel-Jeżewska, and E. Wajnryb, J. Chem. Phys. **144**, 076101 (2016).

[317] S. Kim and S. J. Karrila, *Microhydrodynamics: principles and selected applications* (Courier Corporation, 2013).

[318] B. Cichocki, M. L. Ekiel-Jeżewska, and E. Wajnryb, J. Chem. Phys. **136**, 071102 (2012), http://dx.doi.org/10.1063/1.3689842 .

[319] A. Chakrabarty, A. Konya, F. Wang, J. V. Selinger, K. Sun, and Q.-H. Wei, Phys. Rev. Lett. **111**, 160603 (2013).

[320] B. Wang, J. Kuo, S. C. Bae, and S. Granick, Nat. Mater. **11**, 481 (2012).

[321] B. J. Berne and R. Pecora, *Dynamic Light Scattering: With Applications to Chemistry, Biology, and Physics*, Dover Books on Physics Series (Dover Publications, 2000).